Analytical Modelling of Self-Powered Electromechanical Piezoelectric Bimorph Beams with Multidirectional excitation

M. F. Lumentut , I. M. Howard

Department of Mechanical Engineering,
Curtin University, Australia

Abstract
Unused mechanical energies can be found in numerous ambient vibration sources in industry including rotating equipment, vehicles, aircraft, piping system, fluid flow, and even external movement of the human body. A portion of the vibration energy can be recovered using piezoelectric transduction and stored for subsequent smart system utilisation for applications including powering wireless sensor devices for health condition monitoring of rotating machines and defence communication technology. The vibration environment in the considered application areas is varied and often changes over time and can have components in three perpendicular directions, simultaneously or singularly. This paper presents the development of analytical methods for modelling of self-powered cantilevered piezoelectric bimorph beams with tip mass under simultaneous longitudinal and transverse input base motions utilising the weak and strong forms of Hamiltonian's principle and space- and time-dependent eigenfunction series which were further formulated using orthonormalisation. The reduced constitutive electromechanical equations of the cantilevered piezoelectric bimorph were subsequently analysed using Laplace transforms and frequency analysis to give multi-mode frequency response functions. The validation between theoretical and experimental results at the single mode of eigenfunction solutions reduced from multi-mode FRFs was also given.

Keywords: Microelectromechanical system; piezoelectric; energy harvesting; smart sensor; Hamiltonian; strong, weak and closed forms; vibration.

1. Introduction

The investigation of energy conversion techniques utilising ambient vibration has been of great interest for many researchers for at least the past decade. Although most developments of embedded piezoelectric structures have focused on applications of crack detection using screw dislocation and inclusion techniques [1], [2] and health condition monitoring [3] and control system [4], the recent applications of piezoelectric devices have also included the conversion of ambient vibration into low electrical power. The energy extracted from vibrating devices and structures can be utilised for powering electronic devices, supplying direct current into rechargeable batteries or electrical power storage devices. One of many applications being considered is for powering smart wireless sensor devices. The usage of piezoelectric material in the application of energy conversion requires knowledge of analytical methods, circuit components, material properties and geometrical structure. An extensive review of energy harvesting devices has been discussed by [5] using electrostatic, electromagnetic and piezoelectric transductions. It is important to note here that the overall inherent mechanism of transductions as shown in the simple diagram in Figure 1 depends on the material design, the

nature of the vibration environment and strategies to increase the power through tuning the mechanical and electrical systems in order to maximise the power for the smart wireless sensor systems [6]. The major benefits of piezoelectric transduction have shown reasonable prospect for self-diagnostic detection of aircraft sensor networks, microelectromechanical system design, compact configuration, high sensitivity with respect to low input mechanical vibration and is suitable to be used as a patch or embedded with other substructures as compared to other transduction methods [7]-[9]. The summary of the three major transductions have advantages and disadvantages as given in Table 1.

The piezoelectric bimorph beam represents a useful candidate for power harvesting as relatively high strain fields can be induced as a consequence of the input vibration producing the resulting electrical field. The resultant extracted electrical energy can be optimised by utilising an electronic circuit capable of supplying the direct current into a rechargeable battery for the usage of wireless sensor communication as shown in [10]. Moreover, there have been numerous extensive analytical studies of electromechanical piezoelectric systems associated with experimental validations. Smits and Choi [11] and Wang et al. [12] derived an analytical solution for the static condition of the bending piezoelectric bimorph beam. However, their analytical methods cannot be applied to the dynamic piezoelectric harvester due to the required coupled electromechanical response. Roundy and Wright [13] investigated the analytical solution using the electrical equivalent of the electromechanical transverse bending form for powering electrical devices but it was limited to the single mode. Some other investigations used analytical methods limited to the single mode of Rayleigh-Ritz's analytical approach as shown by duToit et al. [14]. The normalised single mode dynamic equation of piezoelectric power harvesting using non-dimensional parameters of dynamic functions was shown by [15] and the multi-mode frequency response using the closed-form method of the piezoelectric bimorph was derived by [16]. The parametric consideration of the micromechanical piezoelectric unimorph beam using the Rayleigh-Ritz method with condensed matrix equation form was shown by Goldschmidtboeing and Woias [17]. The study of the optimal piezoelectric patch shape using finite element methods has been discussed by Friswell and Adhikari [18]. Sun et al. [19] discussed the single mode dynamic response of the piezoelectric nanostructure power harvesting. Harigai et al. [20] discussed the experimental study of cantilevered micro-piezoelectric unimorph patched onto a silicon substructure under input transverse vibration from an electromagnetic mechanical shaker. The electromechanical dynamic equation derived using the weak form of Hamiltonian's principle introduced by Lumentut and Howard [21], [22]

was used to formulate complete forms of multi-mode frequency response functions using the normalised Ritz eigenfunction form. Furthermore, the theoretical method was validated with experimental results by considering the two input base motion exciting the piezoelectric bimorph to stimulate polar power harvesting [23].

This paper presents a novel analytical method of modelling the electromechanical dynamic equation of a piezoelectric bimorph beam under two input base acceleration using the weak and strong forms of Hamiltonian's principle. The mathematical derivations of electromechanical dynamic equations are analysed to give the piezoelectric couplings due to polarity-electric field, the bending transverse and longitudinal stiffness coefficients due to the stress fields, mass moment of inertias due to velocities of bimorph element including tip mass element, internal capacitance due to permittivity, inertia input loads due to base excitations and electrical charge output. The strain and polarity-electric field depends not only on the physical material characteristics and its geometry but also on the polarity sign conventions. New coupling superposition methods for electrical series and parallel connections are shown in order to illustrate the clear mathematical concepts and theories of forward and backward piezoelectric coupling coefficients under input dynamic excitations (longitudinal and transverse motions). Moreover, the electromechanical weak and closed form methods provide deep analytical insight of the system behaviour. The weak form analytical approach derived from the strong form solution was further derived using the Ritz method by introducing an eigenvector function (Ritz coefficient) and space- and time-dependent Ritz eigenfunction series which were further formulated using orthonormalisation. The closed-form boundary value method derived from the strong-form method was further formulated using a direct analytical solution with orthonormalisation by introducing the space- and time-dependent eigenfunction series into boundary conditions. The closed-form solution was shown to provide accurate results over the frequency response domain because of its convergence at any particular mode of interest whereas the weak form can give similar results with the closed form provided that the typical mode shapes and number of modes are chosen correctly in order to meet the convergence criteria. The normalised electromechanical piezoelectric bimorph beam with a tip mass is further analysed using Laplace transformation to obtain the frequency response functions (FRFs) of the dynamic velocity, voltage, current and power harvesting. Sample theoretical and experimental comparison results from the frequency response analysis of the bimorph with parallel electrical connections are also presented.

2. Constitutive Electromechanical Dynamic Equations

The electrical enthalpy of the piezoelectric material in tensor notation based on continuum thermodynamics condensed using Voigt's notation and then further reduced using Einstein's summation convention gives [6], [24]-[27],

$$\hat{H}(\varepsilon_1, E_3) = \frac{1}{2}\overline{Q}_{11}^{E}\varepsilon_1^{2} - e_{31}E_3\varepsilon_1 - \frac{1}{2}\varsigma_{33}^{\varepsilon}E_3^{2}, \tag{1}$$

The above formulations assume the adiabatic and isothermal processes. Here $\overline{Q}_{11}^{E}$, e_{31}, $\varsigma_{33}^{\varepsilon}$, E_3, σ_1, ε_1 and D_3 represent the piezoelectric elastic coefficient at constant electric field, piezoelectric coefficient, permittivity under constant strain, electric field, stress, strain and electric displacement, respectively. Some notations from equation (1) have been adapted in this research for further mathematical derivations.

The kinematic equations of the infinitesimal piezoelectric beam with two input base motions were developed to formulate the energies of the structure element. The effect of two input base motions of the structure not only affects the strain fields of each layer of the piezoelectric bimorph but also affects the piezoelectric couplings to create the electrical force and moment of the piezoelectric layers when the series and parallel connections are chosen for the bimorph [6]. In Figure 2, let point *p* represents an arbitrary point on the undeformed beam structure with positions *x* and *z* in the fixed frame of reference *oXZ* defined by $\mathbf{R}^{\mathbf{op}} = x\mathbf{e_1} + z\mathbf{e_3}$. The base support at point *o* moves to point *o'* in vector $\mathbf{R_{base}}$ where point *p* also moves to point *p'* for the frame of reference of *o' xz* as indicated. The position vector $\mathbf{R_{base}}$ has the same magnitude as vector $\mathbf{R}^{\mathbf{pp'}}$ by defining $\mathbf{R_{base}} = u_{base}\mathbf{e_1} + w_{base}\mathbf{e_3}$. As the base support undergoes motions, point *p'* undergoes deformation in the longitudinal extension and transverse bending forms as indicated by moving to point *p"*. The position of point *p"* has a condition of absolute displacement with respect to frame of reference *oXZ* defined by $\mathbf{w_{abs}}$ and $\mathbf{u_{abs}}$, where $\mathbf{w_{abs}} = (w_{base} + w_{rel})\mathbf{e_3}$ and $\mathbf{u_{abs}} = (u_{base} + u_{rel})\mathbf{e_1}$. To obtain position vector $\mathbf{R}^{\mathbf{pp''}}$, $\mathbf{R}^{\mathbf{op''}}$ needs to be defined as,

$$\mathbf{R}^{\mathbf{op''}} = \left(x + u_{abs} - z\frac{\partial w_{rel}(x,t)}{\partial x}\right)\mathbf{e_1} + (w_{abs} + z)\mathbf{e_3}. \tag{2}$$

As the position vector $\mathbf{R}^{\mathbf{op}}$ is defined, the position vector $\mathbf{R}^{\mathbf{pp''}}$ can be obtained and differentiated with respect to time to give,

$$\dot{\mathbf{R}}^{\mathbf{pp''}}(x,z,t) = \dot{\mathbf{R}}^{\mathbf{op''}} - \dot{\mathbf{R}}^{\mathbf{op}} = (\dot{u}_{rel}(x,t) + \dot{u}_{base}(t))\mathbf{e_1} - \frac{\partial \dot{w}_{rel}(x,t)}{\partial x}\mathbf{e_2} \times z\mathbf{e_3} + (\dot{w}_{base}(t) + \dot{w}_{rel}(x,t))\mathbf{e_3}. \tag{3}$$

$\dot{\mathbf{R}}^{pp''}$ is defined as the absolute velocity of point p'' with respect to the fixed frame of reference *oXZ*. The geometrical position of the bimorph tip mass can be measured from the fixed frame of reference *oXZ* to the deformation point and this vector can be differentiated with respect to time to give the absolute velocity of the tip mass in terms of the moving base support as,

$$\dot{\mathbf{R}}^{\mathbf{m}}\left(L, r_{gm} \in \{x_{gm}, z_{gm}\}, t\right) = \left(\dot{u}_{rel}(L,t) + \dot{u}_{base}(t)\right)\mathbf{e_1} - \frac{\partial \dot{w}_{rel}(L,t)}{\partial x}\mathbf{e_2} \times \left(x_{gm}\mathbf{e_1} + z_{gm}\mathbf{e_3}\right) + \left(\dot{w}_{base}(t) + \dot{w}_{rel}(L,t)\right)\mathbf{e_3}. \quad (4)$$

In this case, the centre of gravity of the tip mass was assumed to coincide with the end of the piezoelectric bimorph $x = L$, where x_{gm} and z_{gm} represent the distance from the arbitrary element mass $\mathrm{d}m = \rho \mathrm{d}\Gamma$ to the centre of gravity of the tip mass. The position vector $\mathbf{R}^{p'p''}$ specifies the relative displacement due to the moving support base in the fixed reference frame *oXZ*,

$$\mathbf{R}^{p'p''}(x,z,t) = \mathbf{R}^{pp''} - \mathbf{R}^{pp'} = \left(u_{rel} - z\frac{\partial w_{rel}}{\partial x}\right)\mathbf{e_1} + w_{rel}(x,t)\mathbf{e_3}. \quad (5)$$

We note that, $\mathbf{R}^{p'p''}$ can be further differentiated with respect to *x* to give the strain field of the element structure,

$$\varepsilon_{xx} = \varepsilon_1 = \frac{\partial\left(\mathbf{R}^{p'p''} \cdot \mathbf{e_1}\right)}{\partial x} = \frac{\partial u_{rel}}{\partial x} - z\frac{\partial^2 w_{rel}}{\partial x^2} = \varepsilon_1^{(0)} - z\varepsilon_1^{(1)}. \quad (6)$$

Here Hamiltonian's principle can be restricted to the particular form of the constitutive electromechanical dynamic equation of the piezoelectric bimorph beam with brass shim substructure and tip mass giving [6],

$$\int_{t_1}^{t_2} \delta\left(L_a + W_f\right)\mathrm{d}t = \int_{t_1}^{t_2}\left(\sum_{k\in m}\delta KE^{(k)} + \delta KE_{tip} - \sum_{k\in p}\delta \hat{H}^{(k)} - \delta PE^{subs} + \sum_{i=1}^{n}\delta W_f{}^{(i)}\right)\mathrm{d}t = 0,\ \forall m \in \{1,2,3\}, p \in \{1,3\} \subset \mathrm{d}\Gamma. \quad (7)$$

Each term from equation (7) can be written in terms of the kinetic energy *KE* for every layer of the bimorph including tip mass, potential energy *PE* from centre brass shim or substructure, electrical enthalpy energy $\hat{H}$ from piezoelectric material at the lower and upper layers and applied mechanical work due to the input base excitations and electrical work due to electrical charge output W_f. Superscripts *k* and *i* indicate the layers of bimorph and input inertia mechanical forces (input base excitations). It is noted that the electrical enthalpy can be stated as, $\delta\hat{H} = \delta PE^{p} - \delta WE^{p}$ which implies the potential energy and electrical energy from the piezoelectric layers. The geometry of the piezoelectric bimorph beam with the tip mass can be modelled as shown in Figure 3. Essentially, the functional forms from Hamiltonian's principle can be extended using the Lagrangian theorem L_a incorporated with the external mechanical

and electrical works W_f. Each variable categorised in the functional forms L_a and W_f in terms of the mathematical model can be stated as [6],

$$L_a = L_a\left(\dot{w}_{rel}, \dot{u}_{rel}, \dot{w}_{rel}(L), \dot{u}_{rel}(L), \frac{\partial \dot{w}_{rel}}{\partial x}(L), \frac{\partial^2 w_{rel}}{\partial x^2}, \frac{\partial u_{rel}}{\partial x}, E\right), W_f = W_f\left(w_{rel}, u_{rel}, w_{rel}(L), u_{rel}(L), v\right). \quad (8)$$

Equation (8) can be further formulated using total differential equations as,

$$\delta L_a = \frac{\partial L_a}{\partial \dot{w}_{rel}}\delta \dot{w}_{rel} + \frac{\partial L_a}{\partial \dot{u}_{rel}}\delta \dot{u}_{rel} + \frac{\partial L_a}{\partial\left(\frac{\partial \dot{w}_{rel}}{\partial x}\right)}\delta\left(\frac{\partial \dot{w}_{rel}}{\partial x}\right) + \frac{\partial L_a}{\partial \dot{w}_{rel}(L)}\delta \dot{w}_{rel}(L) + \frac{\partial L_a}{\partial \dot{u}_{rel}(L)}\delta \dot{u}_{rel}(L)$$

$$+ \frac{\partial L_a}{\partial\left(\frac{\partial \dot{w}_{rel}}{\partial x}(L)\right)}\delta\left(\frac{\partial \dot{w}_{rel}}{\partial x}(L)\right) + \frac{\partial L_a}{\partial\left(\frac{\partial^2 w_{rel}}{\partial x^2}\right)}\delta\left(\frac{\partial^2 w_{rel}}{\partial x^2}\right) + \frac{\partial L_a}{\partial\left(\frac{\partial u_{rel}}{\partial x}\right)}\delta\left(\frac{\partial u_{rel}}{\partial x}\right) + \frac{\partial L_a}{\partial E}\delta E, \quad (9a)$$

$$\delta W_f = \frac{\partial W_f}{\partial w_{rel}}\delta w_{rel} + \frac{\partial W_f}{\partial u_{rel}}\delta u_{rel} + \frac{\partial W_f}{\partial w_{rel}(L)}\delta w_{rel}(L) + \frac{\partial W_f}{\partial u_{rel}(L)}\delta u_{rel}(L) + \frac{\partial W_f}{\partial v}\delta v. \quad (9b)$$

Corresponding to equations (1), (3), (4), (6), (8) and (9), the reduced Hamiltonian constitutive electromechanical dynamic equation for the piezoelectric bimorph beam with tip mass from equation (7) can be formulated in terms of virtual relative and base displacement forms after applying divergence theorem as [6],

$$\int_{t_1}^{t_2}\left[\int_{\Omega}\left\{-I^{(A,k)}\ddot{u}_{rel}\delta u_{rel} + I^{(C,k)}\frac{\partial^2 \ddot{w}_{rel}}{\partial x^2}\delta w_{rel} - I^{(A,k)}\ddot{w}_{rel}\delta w_{rel} - I^{(A,k)}\ddot{u}_{base}\delta u_{rel} - I^{(A,k)}\ddot{w}_{base}\delta w_{rel}\right.\right.$$

$$+ C_{11}^{(D,k)}\frac{\partial \varepsilon_1^{(0)}}{\partial x}\delta u_{rel} - C_{11}^{(F,k)}\frac{\partial^2 \varepsilon_1^{(1)}}{\partial x^2}\delta w_{rel} - R_{31}^{(G,k)}\frac{\partial v}{\partial x}\delta u_{rel} - R_{31}^{(H,k)}\frac{\partial^2 v}{\partial x^2}\delta w_{rel} + R_{31}^{(G,k)}\frac{\partial u_{rel}}{\partial x}\delta v$$

$$\left.\left. - R_{31}^{(H,k)}\frac{\partial^2 w_{rel}}{\partial x^2}\delta v + S_{33}^{(k)}v\delta v\right\}\mathrm{d}x\mathrm{d}y + q\delta v - I_{tip}^{(A)}\ddot{u}_{rel}(L)\delta u_{rel}(L) - I_{tip}^{(C)}\frac{\partial \ddot{w}_{rel}}{\partial x}(L)\delta\frac{\partial w_{rel}}{\partial x}(L)\right.$$

$$- I_{tip}^{(A)}\ddot{w}_{rel}(L)\delta w_{rel}(L) - I_{tip}^{(A)}\ddot{u}_{base}(L)\delta u_{rel}(L) - I_{tip}^{(A)}\ddot{w}_{base}(L)\delta w_{rel}(L)$$

$$- \oint_S n_x N_{xx}^{(D,k)}\delta u_{rel}\mathrm{d}S + \oint_S n_x\frac{\partial M_{xx}^{(F,k)}}{\partial x}\delta w_{rel}\mathrm{d}S - \oint_S n_x M_{xx}^{(F,k)}\frac{\partial \delta w_{rel}}{\partial x}\mathrm{d}S + \oint_S n_x R_{31}^{(G,k)}v\delta u_{rel}\mathrm{d}S$$

$$\left. + \oint_S n_x R_{31}^{(H,k)}\frac{\partial v}{\partial x}\delta w_{rel}\mathrm{d}S - \oint_S n_x R_{31}^{(H,k)}v\frac{\partial \delta w_{rel}}{\partial x}\mathrm{d}S - \oint_S I^{(C,k)}n_x\frac{\partial \ddot{w}_{rel}}{\partial x}\delta w_{rel}\mathrm{d}S\right]\mathrm{d}t = 0. \quad (10)$$

The superscripts *A*, *C*, *D*, *F*, *G* and *H* indicate properties of mass moment of inertias for first and third terms (rotary inertia), stiffness coefficients for longitudinal extension and transverse bending, piezoelectric couplings for longitudinal extension and transverse bending, respectively. All coefficients from equation (10) can be put forwarded in the next section. It is noted that in the variational method, equation (10) reduced from the extremum of functional

form with integration by two instants of time t_1 and t_2 for all domains in L_a and W_f implied space of function for all independent variables of relative longitudinal $u_{rel}(x,t) \in \mathrm{C}^2[0,L] \subset \Omega \subset \mathrm{R}^3$ and relative transverse displacements $w_{rel}(x,t) \in \mathrm{C}^4[0,L] \subset \Omega \subset \mathrm{R}^3$ associated with electric potential $\varphi(z,t) = \Phi(z)v(t) \in E_3 \in \left\{ \mathrm{C}^1\left[-\frac{h_s}{2} - h_p, -\frac{h_s}{2} \right] \cup \mathrm{C}^1\left[\frac{h_s}{2}, \frac{h_s}{2} + h_p \right] \right\} \subset \Omega \subset \mathrm{R}^3$ in terms of actual forces and moments of the mechanical and electrical fields for the piezoelectric element as prescribed in the partial differential electromechanical dynamic equations in domain $\mathrm{d}\Omega$ including the boundary conditions on the vector surface $\mathrm{d}S$ in terms of the divergence theorem. In this case, the reduced equation must fulfill the mathematical lemma of the variational method of duBois-Reymond's theorem for each virtual displacement field.

2.1. Determining stiffness coefficients for the piezoelectric bimorph interlayer

The elastic stiffness coefficients of the piezoelectric bimorph C_{11} from equation (10) are formulated according to the characteristic material properties and the cross section of each layer of bimorph to give,

$$\forall C_{11}^{(n,k)} \in \left[\sum_{k=1}^{3} \int_{h_k}^{h_{k+1}} \overline{Q}_{11}^{(D,k)} \mathrm{d}z \ , \sum_{k=1}^{3} \int_{h_k}^{h_{k+1}} z \overline{Q}_{11}^{(E,k)} \mathrm{d}z \ , \sum_{k=1}^{3} \int_{h_k}^{h_{k+1}} z^2 \overline{Q}_{11}^{(F,k)} \mathrm{d}z \right] \ , \forall k \subset n \in \{D,E,F\} \ . \quad (11a)$$

The piezoelectric bimorph considered here has symmetrical geometry with the same material used for the upper and lower layers with a centre brass shim. The extensional stiffness coefficient of the interlayer of the piezoelectric bimorph can then be written as,

$$C_{11}^{(D,k)} = h_p \overline{Q}_{11}^{(D,1)} + h_s \overline{Q}_{11}^{(D,2)} + h_p \overline{Q}_{11}^{(D,3)} \quad , \quad (11b)$$

where $\overline{Q}_{11}^{(D,1)} = \overline{Q}_{11}^{(D,3)}$. The extensional-bending stiffness coefficient $C_{11}^{(E,k)}$ from equation (11a) tends to be zero due to the symmetrical geometry and material of the bimorph element structure. Therefore, the coefficient $C_{11}^{(E,k)}$ is not shown from equation (10). The bending stiffness coefficient can be formulated as,

$$C_{11}^{(F,k)} = \left(-\frac{{h_s}^3}{24} - \frac{1}{3}\left(-h_p - \frac{h_s}{2} \right)^3 \right) \overline{Q}_{11}^{(F,1)} + \frac{{h_s}^3}{4} \overline{Q}_{11}^{(F,2)} + \left(\frac{1}{3}\left(h_p + \frac{h_s}{2} \right)^3 - \frac{{h_s}^3}{24} \right) \overline{Q}_{11}^{(F,3)} \ . \quad (11c)$$

It should be noted that $\overline{Q}_{11}^{(D,1)} = \overline{Q}_{11}^{(D,3)} = \overline{Q}_{11}^{(F,1)} = \overline{Q}_{11}^{(F,3)}$ and $\overline{Q}_{11}^{(D,2)} = \overline{Q}_{11}^{(F,2)}$ indicate the plane stress-based elastic stiffness at constant electric field for piezoelectric material and plane stress-based elastic stiffness for brass material, respectively.

2.2. Determining forward and backward piezoelectric coupling coefficients

The coefficient R_{31} from equation (10), known as the forward and backward piezoelectric couplings, will be discussed in terms of series and parallel connections of the piezoelectric bimorph. It is noted that the direct effect of the piezoelectric element, developed in potential form, indicates the backward piezoelectric coupling whereas the converse effect of the piezoelectric element gives the forward piezoelectric coupling which is formulated from electrical energy. As the piezoelectric behaviour is reversible, the forward piezoelectric couplings have the same values as the backward piezoelectric couplings. This indicates that the piezoelectric couplings are affected by the electrical force and moment of the piezoelectric layers which depend on the strain fields and the polarity-electric field. In this case, new techniques of formulating the piezoelectric couplings will also be given. The electric field of the piezoelectric bimorph depends on the positive and negative terminals located at the lower and upper surfaces of the piezoelectric element, respectively. Each connection (series and parallel connections) can be arranged into two types of poled configurations i.e. X-poled and Y-Poled which depends on the direction of polarities and strain effect between the piezoelectric benders $k \in \{1,3\}$ (upper element and lower element). At this point, when the piezoelectric element was initially undeformed, the polarisation direction, for example, was in the z-axis called the initial polarised state. When the tensile stress acts perpendicular to the z-axis on the element, the polarisation will behave in the opposite direction to the z-axis. Conversely, when the piezoelectric element is under compressive stress perpendicular with the z-axis, the polarisation will be in the same direction with the z-axis. It means that the change of stress from tensile to compressive or vice versa in the piezoelectric element will result in a reversal of the direction of polarisation [24]. This situation is known as the direct piezoelectric effect where the polarisation is proportional to the stress field and the stress field is also proportional to the strain field or it can be stated in terms of Einstein's summation convention as $P_i = d_{ij}\sigma_j$. This has been reflected in the electrical enthalpy of the piezoelectric formulation [25],[27]. Based on this case, the piezoelectric bimorph under series and parallel connections can be further considered. For example, in series connection shown in Figure 3, when the piezoelectric element undergoes transverse input base motion, by assumption here, the upper and lower layers of the piezoelectric bimorph can respectively deform with the tension and compressive strains and polarisation of the upper layer will then create opposite directions compared with the lower layer (X-poled). It should be noted that the polarisation directions affect mathematically the piezoelectric coefficients due to the stress field on the element structure

whilst the electric field generates electrical voltage. Consequently, the electrical moments at both lower and upper layers will be formed. With the same electrical connection, when the piezoelectric bimorph is under input longitudinal base motion, the upper and lower layers of the bimorph have the same deformation, for example, compressive strain and then the polarization at the upper and lower layers have the same direction (Y-poled), while the electric field will be generating electric voltage to create the electrical force at both the lower and upper layers. This situation exists when the piezoelectric bimorph beam operates under two input base motions which was considered here mathematically by backward and forward coupling superposition of the elastic-polarity field [6]. Smits and Choi [11] and Smits et al. [28] discussed the sign conventions of electric field and piezoelectric coefficient for the series and parallel connections. However, their formulations of the transverse bending bimorph beam only considered the static condition. In this section, the complete piezoelectric couplings due to the effect of electric field and polarity directions are discussed here when the bimorph undergoes two input base motions.

As shown in Figure 5, the piezoelectric bimorph under parallel connection also depends on the input base motions and direction of polarity. The strain fields between the upper and lower layers have similar behaviour with series connection. The difference lies with the polarisation and electric field directions due to the chosen parallel connection of the piezoelectric bimorph. This is achieved at the upper layer of the piezoelectric bimorph under X-poled series connection by applying a strong electric field to direct initial polarisation in the same direction with the lower layer or it can be provided according to the manufacturing process in such a way that the parallel connection can be arranged as shown in Figure 5. In this case, the polarisation tends to show the same directions each other when the tension strains are opposite between the lower and upper layers due to the input transverse base motion. On the other hand, when the piezoelectric bimorph was treated to the input base longitudinal motion, two polarisations at the upper and lower layers tend to give opposite directions due to the compressive strains in the piezoelectric elements, respectively.

In this case, the sign conventions of electric field and piezoelectric coefficient needs to be considered for the series and parallel connections under two input base motions. As assumed here, the polarisation indicates the opposite direction with respect to electric field, with the piezoelectric constant having a resulting negative sign and vice versa. Series connection normally has two wires where one wire attaches to the electrode of the lower layer and one wire attaches to the electrode of the upper layer whereas parallel connection normally has three

wires where one wire connects to the centre shim and two wires are located at the electrodes of the lower and upper layers. It is noted that the common piezoelectric constant produced from the manufacturing company is in the form d_{31} but this can be modified by multiplying the plane stress-based elastic stiffness at constant electric field to give $e_{31} = d_{31}\overline{Q}_{11}^{E}$.

Furthermore, the series connection of the piezoelectric bimorph results in the positive sign of electric field at both the lower and upper layers with the same direction as the positive *z* axis because the piezoelectric bimorph for series connection has a positive terminal at the electrode of the lower layer and a negative terminal at the upper layer. However, the parallel connection indicates a positive sign of the electric field for the lower layer and a negative sign for the upper layer because the piezoelectric bimorph for the parallel connection has a positive terminal at the electrodes of the lower and upper layers and a negative terminal between the centre brass shim [6]. The electric field can be formulated as,

$$E_3^{(n,k)} = -\nabla\varphi(z,t) = \Xi(z)^{(n,k)} v(t) \text{ where } \varphi(z,t) = -(-1)^r \Phi(z) v(t),\ \Xi(z)^{(n,k)} = -(-1)^r \nabla\Phi(z) \quad .(12)$$

It is considered here that $\Phi(z)$ represents the shape function of the electric voltage $v(t)$ and it applies to each layer of the piezoelectric bimorph. $\Xi(z)^{(n,k)}$ is the gradient operator of the electric voltage shape function and subscript *r* refers to 1 or 2 to be used for sign convention. This indicates the change of sign of the electric field due to the terminal connections of the upper and lower electrodes of the piezoelectric bimorph containing the charges normally flowing from positive to negative terminals. The modified piezoelectric constant can be formulated as,

$$\Psi_{31}^{(n,k)} = (-1)^s e_{31}^{(n,k)} \quad . \tag{13}$$

Superscript *s* refers to the change of sign of piezoelectric coefficient due to change of polarisation. The equation (10) for piezoelectric couplings $R_{31}^{(n,k)}$ can be formulated for each outside layer as,

$$\forall R_{31}^{(n,k)} \in \left[\sum_{k \in p} \int_{h_k}^{h_{k+1}} \Psi_{31}^{(G,k)} \Xi(z)^{(G,k)} \mathrm{d}z \ , \sum_{k \in p} \int_{h_k}^{h_{k+1}} z \Psi_{31}^{(H,k)} \Xi(z)^{(H,k)} \mathrm{d}z \right], \forall k \in \{1,3\} \subset n \in \{G, H\}. \tag{14}$$

$R_{31}^{(G,k)}$ represents the backward and forward piezoelectric couplings for the longitudinal extension term and $R_{31}^{(H,k)}$ represents the backward and forward piezoelectric couplings for the transverse bending term. As mentioned previously, the forward piezoelectric couplings indicate equal form with the backward piezoelectric couplings.

Case 1. Series connection. Corresponding to equation (12), the electric voltage $v(t)$ for series connection is considered to provide half the voltage between the electrodes of the piezoelectric bimorph. Therefore, the shape function of the electric potential can be formulated based on the thickness of each layer of the piezoelectric bimorph to give,

$$\Phi(z)_s^{(n,1)} = \frac{-z-\frac{h_s}{2}}{2h_p} \;, -\frac{h_s}{2}-h_p \le z \le -\frac{h_s}{2} \;;\; \Phi(z)_s^{(n,3)} = \frac{z-\frac{h_s}{2}}{2h_p} \;,\; \frac{h_s}{2} \le z \le \frac{h_s}{2}+h_p . \qquad (15a)$$

a. X-poled due to transverse form where the polarisation has opposite direction. Equation (14) for transverse effect meets the function of polarisation for each layer $k \in \{1,3\}$ due to the conditions of equations (12), (13) and (15a),

$$\left(R_{31}^{(H,k)}\right)_{\text{series}} = \left\{ \Psi_{31}^{(H,k)} \Xi(z)^{(H,k)} \middle|\; s=2, r=2, \forall\; k=1 \subset n \in H \subset \Omega \times \left[-\frac{h_s}{2}-h_p, -\frac{h_s}{2}\right] \subset \Gamma \right\}, \qquad (15b)$$

$$\left(R_{31}^{(H,k)}\right)_{\text{series}} = \left\{ \Psi_{31}^{(H,k)} \Xi(z)^{(H,k)} \middle|\; s=1,\; r=1, \forall\; k=3 \subset n \in H \subset \Omega \times \left[\frac{h_s}{2}, \frac{h_s}{2}+h_p\right] \subset \Gamma \right\}. \qquad (15c)$$

Backward and forward piezoelectric couplings of the X-poled transverse bending form can be formulated using equation (14) resulting in,

$$R_{31(\text{series})}^{(H,k)} = -\frac{e_{31}^{(H,1)}}{2h_p}\left(\frac{{h_p}^2}{2}+\frac{h_p h_s}{2}\right) - \frac{e_{31}^{(H,3)}}{2h_p}\left(\frac{{h_p}^2}{2}+\frac{h_p h_s}{2}\right) = -\frac{e_{31}}{h_p}\left(\frac{{h_p}^2}{2}+\frac{h_p h_s}{2}\right). \qquad (15d)$$

b. Y-poled due to longitudinal extension where the polarisation has the same direction. Equation (14) for longitudinal effect meets the function of polarisation for each layer due to the condition of equations (12), (13) and (15a),

$$\left(R_{31}^{(G,k)}\right)_{\text{series}} = \left\{ \Psi_{31}^{(G,k)} \Xi(z)^{(G,k)} \middle|\; s=2, r=2, \forall\; k=1 \subset n \in G \subset \Omega \times \left[-\frac{h_s}{2}-h_p, -\frac{h_s}{2}\right] \subset \Gamma \right\}, \qquad (15e)$$

$$\left(R_{31}^{(G,k)}\right)_{\text{series}} = \left\{ \Psi_{31}^{(G,k)} \Xi(z)^{(G,k)} \middle|\; s=2,\; r=1, \forall\; k=3 \subset n \in G \subset \Omega \times \left[\frac{h_s}{2}, \frac{h_s}{2}+h_p\right] \subset \Gamma \right\}. \qquad (15f)$$

Backward and forward piezoelectric couplings of the Y-poled longitudinal extension can be formulated using equation (14) resulting in,

$$R_{31}^{(G,k)} = \frac{h_p e_{31}^{(G,1)}}{2h_p} + \frac{h_p e_{31}^{(G,3)}}{2h_p} = e_{31} \qquad . \qquad (15g)$$

Case 2. Parallel connection. The electric voltage $v(t)$ for parallel connection is considered to give one voltage between the electrodes of the piezoelectric bimorph. This means that the shape function of the electric potential is divided by a factor of one. Therefore, the shape

function of electric potential can be formulated based on the thickness of each layer of the piezoelectric bimorph, to give,

$$\Phi(z)_p^{(n,1)} = \frac{-z-\frac{h_s}{2}}{h_p} \;,\; -\frac{h_s}{2}-h_p \le z \le -\frac{h_s}{2} \quad ; \quad \Phi(z)_p^{(n,3)} = \frac{z-\frac{h_s}{2}}{h_p} \;,\; \frac{h_s}{2} \le z \le \frac{h_s}{2}+h_p \,. \tag{16a}$$

a. X-poled due to longitudinal extension form where the polarisation has opposite direction. Equation (14) for longitudinal effect meets the function of polarisation for each layer due to the condition of equations (12), (13) and (16a),

$$\left(R_{31}^{(G,k)}\right)_{\text{parallel}} = \left\{ \Psi_{31}^{(G,k)} \Xi(z)^{(G,k)} \mid s=2,\, r=2, \forall\, k=1 \subset n \in G \subset \Omega \times \left[-\frac{h_s}{2}-h_p, -\frac{h_s}{2}\right] \subset \Gamma \right\}, \tag{16b}$$

$$\left(R_{31}^{(G,k)}\right)_{\text{parallel}} = \left\{ \Psi_{31}^{(G,k)} \Xi(z)^{(G,k)} \mid s=1,\, r=2, \forall\, k=3 \subset n \in G \subset \Omega \times \left[\frac{h_s}{2}, \frac{h_s}{2}+h_p\right] \subset \Gamma \right\}. \tag{16c}$$

Backward and forward piezoelectric coupling of the X-poled longitudinal extension can be formulated using equation (14) resulting in,

$$R_{31(\text{parallel})}^{(G,k)} = e_{31}^{(G,1)} + e_{31}^{(G,3)} = 2e_{31}. \tag{16d}$$

b. Y-poled due to transverse bending form where the polarisation has the same direction. Because the polarisations have the same direction as the global direction of the electric field in the z direction, the backward and forward piezoelectric coefficients in both layers have conditions as,

$$\left(R_{31}^{(H,k)}\right)_{\text{parallel}} = \left\{ \Psi_{31}^{(H,k)} \Xi(z)^{(H,k)} \mid s=2, r=2, \forall\, k=1 \subset n \in H \subset \Omega \times \left[-\frac{h_s}{2}-h_p, -\frac{h_s}{2}\right] \subset \Gamma \right\}, \tag{16e}$$

$$\left(R_{31}^{(H,k)}\right)_{\text{parallel}} = \left\{ \Psi_{31}^{(H,k)} \Xi(z)^{(H,k)} \mid s=2,\, r=2, \forall\, k=3 \subset n \in H \subset \Omega \times \left[\frac{h_s}{2}, \frac{h_s}{2}+h_p\right] \subset \Gamma \right\}. \tag{16f}$$

The piezoelectric coupling of the Y-poled transverse bending form can be formulated using equation (14) resulting in,

$$R_{31(\text{parallel})}^{(H,k)} = -\frac{e_{31}^{(H,1)}}{h_p}\left(\frac{{h_p}^2}{2}+\frac{h_p h_s}{2}\right) - \frac{e_{31}^{(H,3)}}{h_p}\left(\frac{{h_p}^2}{2}+\frac{h_p h_s}{2}\right) = -\frac{2e_{31}}{h_p}\left(\frac{{h_p}^2}{2}+\frac{h_p h_s}{2}\right). \tag{16g}$$

2.3. Determining internal capacitance of the piezoelectric bimorph

The internal capacitance per unit area of piezoelectric bimorph from equation (10) can be formulated as,

$$\forall S_{33}^{(k)} = \left[\sum_{k \in p} \int_{h_k}^{h_{k+1}} \Xi(z)^{(k)} \varsigma_{33}^{(k)} \Xi(z)^{(k)} \mathrm{d}z \right], \; \forall k \in \{1,3\}. \tag{17a}$$

Case 1. Series connection. The capacitance of the piezoelectric element was formulated in equation (17a). The summation of capacitances between the upper and lower layers of the piezoelectric bimorph has a factor of 1/2. The capacitance for series connection can be formulated as,

$$S_{33}^{(k)} = \frac{h_p \varsigma_{33}^{(1)}}{4{h_p}^2} + \frac{h_p \varsigma_{33}^{(3)}}{4{h_p}^2} = \frac{\varsigma_{33}}{2h_p}. \tag{17b}$$

It should be noted that the upper and lower layers of the piezoelectric bimorph have the same material and geometrical structure, thus the permittivity of the piezoelectric component gives , $\varsigma_{33}^{(1)} = \varsigma_{33}^{(3)} = \varsigma_{33}$.

Case 2. Parallel connection. The summation of capacitances between the upper and lower layers of the piezoelectric bimorph has a factor of 2. At this point, the capacitance of the piezoelectric element for parallel connection can be formulated as,

$$S_{33}^{(k)} = \frac{h_p \varsigma_{33}^{(1)}}{{h_p}^2} + \frac{h_p \varsigma_{33}^{(3)}}{{h_p}^2} = \frac{2\varsigma_{33}}{h_p}. \tag{17c}$$

The capacitance can affect the electric displacement as a converse effect where it depends on the geometrical structure of the piezoelectric element and permittivity.

2.4. Determining mass moment of inertias of the piezoelectric bimorph and tip mass

The mass moment of inertias per unit area are formulated according to the characteristic materials and the cross section of each layer of bimorph,

$$\forall I^{(n,k)} \in \left[\sum_{k=1}^{3} \int_{h_k}^{h_{k+1}} \rho^{(A,k)} \mathrm{d}z \ , \sum_{k=1}^{3} \int_{h_k}^{h_{k+1}} z\rho^{(B,k)} \mathrm{d}z \ , \sum_{k=1}^{3} \int_{h_k}^{h_{k+1}} z^2 \rho^{(C,k)} \mathrm{d}z \right], \ \forall k \subset n \in \{A,B,C\}. \tag{18a}$$

The zero-th mass moment of inertia per unit area gives,

$$I^{(A,k)} = h_p \rho^{(A,1)} + h_s \rho^{(A,2)} + h_p \rho^{(A,3)} \ . \tag{18b}$$

The first mass moment of inertia per unit area $I^{(B,k)}$ from equation (18a) tends to be zero, since the centroid of the section is located at the neutral axis of the bimorph which has symmetrical geometry and the same material of the bimorph element structure. Therefore, the coefficient $I^{(B,k)}$ is not shown from equation (10). Furthermore, the second mass moment of inertia or rotary inertia per unit area is formulated as,

$$I^{(C,k)} = \left(-\frac{{h_s}^3}{24} - \frac{1}{3}\left(-h_p - \frac{h_s}{2} \right)^3 \right) \rho^{C,1} + \frac{{h_s}^3}{4} \rho^{C,2} + \left(\frac{1}{3}\left(h_p + \frac{h_s}{2} \right)^3 - \frac{{h_s}^3}{24} \right) \rho^{C,3} \ . \tag{18c}$$

The mass densities $\rho^{(C,1)}$ and $\rho^{(C,3)}$ are assumed to have the same material located on the lower and upper piezoelectric layers, respectively. It should be noted that $\rho^{(A,1)}=\rho^{(A,3)}=\rho^{(C,1)}=\rho^{(C,3)}$ and $\rho^{(A,2)}=\rho^{(C,2)}$.

The tip mass moment of inertia is also formulated as,

$$\forall I_{tip}^{(m)} \in \left[\int_{\Gamma} \rho_{tip}^{(A)} \mathrm{d}x\mathrm{d}y\mathrm{d}z \, , \int_{\Gamma} z\rho_{tip}^{(B)} \mathrm{d}x\mathrm{d}y\mathrm{d}z \, , \int_{\Gamma} \left(x_{gm}{}^2 + z_{gm}{}^2 \right) \rho_{tip}^{(C)} \mathrm{d}x\mathrm{d}y\mathrm{d}z \right] , \forall m \in \{A,B,C\}. \quad (19a)$$

It is noted that the third integral term implies the second mass moment of inertia for the arbitrary geometric shapes where further detail can be found in Beer and Johnston [29]. Figure 3 indicated an example shape of the tip mass where the zero-th tip mass moment of inertia is formulated,

$$I_{tip}^{(A)} = \left(h_{tip} l_{tip} - \left(2h_p + h_s \right) l_b \right) s_{tip} \rho_{tip}^{(A)} \, . \quad (19b)$$

The first mass moment of inertia $I_{tip}^{(B)}$ tends to be zero because the geometric shape only has one centre of gravity where each moment with respect to the centroid has equal magnitude. The second tip mass moment of inertia is known as rotary inertia at the centre of gravity of the tip mass which is assumed to coincide with the end length of the piezoelectric bimorph beam. This results in,

$$I_{tip}^{(C)} = \left\{ \left(\frac{\left(l_{tip}^{2} + h_{tip}^{2} \right)}{12} + \bar{x}_1{}^2 - \frac{\left(\left(2h_p + h_s \right)^2 + l_b{}^2 \right)}{12} - \bar{x}_2{}^2 \right) \left(l_{tip} h_{tip} - \left(2h_p + h_s \right) l_b \right) \right\} s_{tip} \rho_{tip}^{(C)} \, , \quad (19c)$$

where $\bar{x}_1 = x_g - l_{tip}/2$, $\bar{x}_2 = x_g - l_b/2$ and x_g is the centre of gravity of geometry of the tip mass.

3. The Strong Form of Electromechanical Dynamic Equation

As prescribed in equation (10), parameters of virtual relative base displacements and electrical potential forms can be separated in terms of partial differential dynamic equations for extensional, transverse and electrical fields to formulate the strong form of Hamiltonian constitutive electromechanical dynamic equation. In this case, there are three constitutive electromechanical equations of the cantilevered piezoelectric bimorph beam associated with moving virtual displacement fields of δu_{rel}, δw_{rel}, $\delta u_{rel}(L)$, $\partial w_{rel}/\partial x(L)$ and δv.

The first constitutive electromechanical dynamic equation in extensional form in terms of virtual relative longitudinal displacement field δu_{rel} reduced from equation (10) can be formulated as,

$$\delta u_{rel}(x,t) \quad : \quad -\hat{I}^{(A,k)}\ddot{u}_{rel} - \hat{I}^{(A,k)}\ddot{u}_{base} + \hat{C}_{11}^{(D,k)}\frac{\partial \varepsilon_1^{(0)}}{\partial x} - R_{31}^{(G,k)}\frac{\partial v}{\partial x} = 0, \tag{20a}$$

It is noted that the symbol ^ indicates the modified parameter after integrating with respect to *y* and the divergence theorem from the nineteenth and twenty first terms in equation (10) can also be modified. The boundary condition can be stated as,

$$\delta u_{rel}(L,t) \quad : \quad -I_{tip}^{(A)}\ddot{u}_{base}(t) - I_{tip}^{(A)}\ddot{u}_{rel}(L) - \hat{C}_{11}^{(D,k)}\frac{\partial u_{rel}}{\partial x} + \hat{R}_{31}^{(G,k)}v = 0,$$

and $u_{rel}(0,t) = 0$. (20b)

It should be noted that the fourth term of equation (20a) is zero because the electric voltage is only a function of time. However, equation (20a) can be used to formulate the weak form of the Hamiltonian constitutive electromechanical dynamic equation. The second constitutive electromechanical dynamic equation for transverse bending form in terms of the virtual relative transverse displacement field δw_{rel} reduced from equation (10) can be formulated as,

$$\delta w_{rel}(x,t) \quad : \quad \hat{I}^{(C,k)}\frac{\partial^2 \ddot{w}_{rel}}{\partial x^2} - \hat{I}^{(A,k)}\ddot{w}_{rel} - \hat{I}^{(A,k)}\ddot{w}_{base} - \hat{C}_{11}^{(F,k)}\frac{\partial^2 \varepsilon_1^{(1)}}{\partial x^2} - \hat{R}_{31}^{(H,k)}\frac{\partial^2 v}{\partial x^2}\delta w_{rel} = 0. \tag{21a}$$

The symbol ^ indicates the modified parameter after integrating with respect to *y*. The boundary condition can be stated after modifying the divergence theorem from the twentieth, twenty first, twenty third, twenty fourth and twenty fifth terms in equation (10) as,

$$\delta w_{rel}(L,t) \quad : \quad -I_{tip}^{(A)}\ddot{w}_{base}(t) - I_{tip}^{(A)}\ddot{w}_{rel}(L) - \hat{I}^{(C,k)}\frac{\partial \ddot{w}}{\partial x}(L) + \hat{C}_{11}^{(F,k)}\frac{\partial}{\partial x}\left(\frac{\partial^2 w_{rel}}{\partial x^2}\right)(L) + \hat{R}_{31}^{(H,k)}\frac{\partial v}{\partial x} = 0,$$

$$\frac{\partial \delta w_{rel}}{\partial x}(L,t) \quad : \quad -I_{tip}^{(C)}\frac{\partial \ddot{w}_{rel}}{\partial x}(L) - \hat{C}_{11}^{(F,k)}\frac{\partial^2 w_{rel}}{\partial x^2}(L) - \hat{R}_{31}^{(H,k)}v = 0 \quad , \tag{21b}$$

$$w_{rel}(0,t) = 0 \quad , \quad \frac{\partial w_{rel}}{\partial x}(0,t) = 0.$$

It should be noted that the fifth term of equation (21a) is zero because the electric voltage is a function of time. However, equation (21a) can be modified to formulate the weak form of the Hamiltonian constitutive electromechanical dynamic equation. The third constitutive dynamic equation for electrical potential in terms of the virtual electrical potential field, $\delta v(t)$ can be formulated as,

$$\delta v \;:\; \int_0^L \left(\hat{R}_{31}^{(G,k)} \frac{\partial u_{rel}}{\partial x} - \hat{R}_{31}^{(H,k)} \frac{\partial^2 w_{rel}}{\partial x^2} + \hat{S}_{33}^{(k)} v \right) \mathrm{d}x + q = 0 . \tag{22}$$

As prescribed by equation (10), the form of the electromechanical dynamic equation represents the electromechanical strong form of Hamiltonian's theorem as shown in equations (20a)-(22). Since the strong form method includes quite tedious derivations to give the electromechanical frequency response function response, the closed-form boundary value method shown in section 5, can be further reduced by using the strong form method.

In the next section, the weak form of the Hamiltonian electromechanical dynamic equations will be formulated from the general and normalised Ritz methods. Since the Ritz method is viewed as an analytical approach, this method can give the same results as the closed-form provided that the space-dependent eigenfunction form from the normalised Ritz method is chosen correctly with the space-dependent eigenfunction form having the same form as the closed-form solution [6].

4. The Weak Solution form of Electromechanical Dynamic Equation

The weak form of the Hamiltonian theorem can also be formulated in terms of the virtual relative extensional δu_{rel} and transverse δw_{rel} displacement fields and virtual electric potential δv to give the analytical integro-partial differential dynamic equation over the length of the piezoelectric bimorph beam. The weak form of Hamiltonian theorem includes the virtual displacements into the calculations of the constitutive electromechanical dynamic equation. In other words, the virtual displacements are assumed to be the non-zero terms. Therefore, the solutions of the dynamic equation in terms of variables fields (u_{rel}, w_{rel}, v) and virtual variables fields (δu_{rel}, δw_{rel}, δv) must be assumed as eigenfunction forms. At this point, the weak form of the Hamiltonian constitutive electromechanical dynamic equation can be formulated by modifying equation (10) and then applying the divergence theorem as [22],[23],

$$\begin{aligned}
&\int_{t_1}^{t_2} \left[\int_{\Omega} \left(C_{11}^{(D,k)} \varepsilon_1^{(0)} \frac{\partial \delta u_{rel}}{\partial x} + C_{11}^{(F,k)} \varepsilon_1^{(1)} \frac{\partial^2 \delta w_{rel}}{\partial x^2} - R_{31}^{(G,k)} v \frac{\partial \delta u_{rel}}{\partial x} + R_{31}^{(H,k)} v \frac{\partial^2 \delta w_{rel}}{\partial x^2} + I^{(A,k)} \ddot{u}_{rel} \delta u_{rel} \right. \right. \\
&- S_{33}^{(k)} v(t) \delta v(t) + I^{(C,k)} \frac{\partial \ddot{w}_{rel}}{\partial x} \frac{\partial \delta (w_{rel})}{\partial x} + I^{(A,k)} \ddot{w}_{rel} \delta w_{rel} - R_{31}^{(G,k)} \frac{\partial u_{rel}}{\partial x} \delta v \\
&\left. \left. + R_{31}^{(H,k)} \frac{\partial^2 w_{rel}}{\partial x^2} \delta v + I^{(A,k)} \ddot{u}_{base} \delta u_{rel} + I^{(A,k)} \ddot{w}_{base} \delta w_{rel} \right) \mathrm{d}x \mathrm{d}y - q \delta v + I_{tip}^{(A)} \ddot{u}_{rel}(L) \delta u_{rel}(L) \right. \\
&+ I_{tip}^{(C)} \frac{\partial \ddot{w}_{rel}}{\partial x}(L) \frac{\partial \delta w_{rel}}{\partial x}(L) + I_{tip}^{(A)} \ddot{u}_{base} \delta u_{rel}(L) + I_{tip}^{(A)} \ddot{w}_{base} \delta w_{rel}(L) + I_{tip}^{(A)} \ddot{w}_{rel}(L) \delta w_{rel}(L)
\end{aligned}$$

$$+\oint_S\left(-n_x N_{xx}^{(D,k)}\delta u_{rel}+n_x\frac{\partial M_{xx}^{(F,k)}}{\partial x}\delta w_{rel}-n_x M_{xx}^{(F,k)}\frac{\partial\delta w_{rel}}{\partial x}-I^{(C,k)}n_x\frac{\partial\ddot{w}_{rel}}{\partial x}\delta w_{rel}\right)\mathrm{d}S\Bigg]\mathrm{d}t=0\,. \quad (23)$$

The weak form of Hamiltonian's principle can also be obtained alternatively in terms of equations (20a)- (22) by applying the variational principle. It should be noted that equations (10) and (23) can be used to formulate the Rayleigh and Euler-Bernoulli piezoelectric bimorph beams. The Rayleigh beam only considered the rotary inertias of the piezoelectric bimorph. The Euler-Bernoulli piezoelectric bimorph beam can also be formulated using the same equation by ignoring the rotary inertia of the piezoelectric bimorph. In forthcoming mathematical derivations, this equation will use the rotary inertia of the piezoelectric bimorph where this will be easier to neglect once the orthonormality property of electromechanical dynamic equations will be established. It should be noted that the second integral represents the divergence theorem reflecting the boundary conditions on the surface *S* of the bimorph element in the direction n_x of the unit vector normal to the *x*-axis. The second integral is sometimes called the generalised internal force and moment for every element discretisation and these become necessary when the element boundary *S* coincides with boundary of domain **Ω**. The second integral can be a crucial part to be included in equation (23) when using finite element analysis where their existence depends on external loads on certain nodes of the structure. In terms of the analytical approach that is proposed here, the second integral can be ignored because the displacement fields (u_{rel}, w_{rel}) and virtual displacement fields ($\delta u_{rel}, \delta w_{rel}$) reflected from equation (23) were assumed as eigenfunction forms which meet the continuity of mechanical form or strain field and boundary conditions.

The solution form of equation (23) can be expanded using the convergent eigenfunction series forms. This equation can be formulated separately from the longitudinal and transverse forms as discussed further in the next section. As previously mentioned, the effects of input base motions on the bimorph not only affects the mechanical domain (stress and strain fields) but also the electrical domain (electric field and polarity). The solution forms can be prescribed using the space- and time-dependent eigenfunction forms as,

$$w_{rel}(x,t)=\sum_{r=1}^{m}w_r(t)\Psi_r(x) \quad , \quad u_{rel}(x,t)=\sum_{r=1}^{m}u_r(t)\Theta_r(x) \quad . \quad (24)$$

Parameters $\Psi(x)$ and $\Theta(x)$ indicate the space-dependence or mode shapes of the eigenfunction series which can be determined using analytical solution forms for the cantilevered piezoelectric beam with a tip mass where the mode shape will be formulated in Appendix A

and B. It should be noted that these parameters are defined as the independent mode shapes of relative motions to meet the continuity requirements of the mechanical strain field.

Corresponding to equation (24), equation (23) can be formulated according to the eigenfunction series forms. Setting virtual displacement forms $\delta u_{rel}(t)$, $\delta w_{rel}(t), \delta v(t)$ separately can be used to obtain three independent dynamic equations. Parameters of virtual displacements meet the duBois-Reymond's lemma to indicate that only dynamic equations have solutions. At this point, the constitutive electromechanical dynamic equations from equation (23) can be reformulated in matrix form by including the damping coefficients after integration with respect to *y* to give,

$$\begin{bmatrix} M_{qr}^{(u)} & 0 & 0 \\ 0 & M_{qr}^{(w)} & 0 \\ 0 & 0 & 0 \end{bmatrix} \begin{Bmatrix} \ddot{u}_r \\ \ddot{w}_r \\ \ddot{v} \end{Bmatrix} + \begin{bmatrix} C_{qr}^{(u)} & 0 & 0 \\ 0 & C_{qr}^{(w)} & 0 \\ P_r^{(u)} & P_r^{(w)} & P_D \end{bmatrix} \begin{Bmatrix} \dot{u}_r \\ \dot{w}_r \\ \dot{v} \end{Bmatrix} + \begin{bmatrix} K_{qr}^{(u)} & 0 & P_q^{(u)} \\ 0 & K_{qr}^{(w)} & P_q^{(w)} \\ 0 & 0 & R_L \end{bmatrix} \begin{Bmatrix} u_r \\ w_r \\ v \end{Bmatrix} = \begin{bmatrix} -Q_q^{(u)} & 0 & 0 \\ 0 & -Q_q^{(w)} & 0 \\ 0 & 0 & 0 \end{bmatrix} \begin{Bmatrix} \ddot{u}_{base} \\ \ddot{w}_{base} \\ \ddot{v}_{base} \end{Bmatrix}, \quad (25)$$

where,

$$M_{qr}^{(u)} = \int_0^L \hat{I}^{(A,k)} \Theta_q(x) \Theta_r(x) \mathrm{d}x + I_{tip}^{(A)} \Theta_q(L) \Theta_r(L) \quad ,$$

$$M_{qr}^{(w)} = \int_0^L \hat{I}^{(A,k)} \Psi_q(x) \Psi_r(x) \mathrm{d}x + \int_0^L \hat{I}^{(C,k)} \frac{\mathrm{d}\Psi_q(x)}{\mathrm{d}x} \frac{\mathrm{d}\Psi_r(x)}{\mathrm{d}x} \mathrm{d}x + I_{tip}^{(A)} \Psi_q(L) \Psi_r(L) + I_{tip}^{(C)} \frac{\mathrm{d}\Psi_q}{\mathrm{d}x}(L) \frac{\mathrm{d}\Psi_r}{\mathrm{d}x}(L) \ ,$$

$$K_{qr}^{(u)} = \int_0^L \hat{C}_{11}^{(D,k)} \frac{\mathrm{d}\Theta_q(x)}{\mathrm{d}x} \frac{\mathrm{d}\Theta_r(x)}{\mathrm{d}x} \mathrm{d}x \quad , \quad K_{qr}^{(w)} = \int_0^L \hat{C}_{11}^{(F,k)} \frac{\mathrm{d}^2\Psi_q(x)}{\mathrm{d}x^2} \frac{\mathrm{d}^2\Psi_r(x)}{\mathrm{d}x^2} \mathrm{d}x \ ,$$

$$P_r^{(u)} = -\int_0^L \hat{R}_{31}^{(G,k)} \frac{\mathrm{d}\Theta_r(x)}{\mathrm{d}x} \mathrm{d}x \quad , \quad P_r^{(w)} = \int_0^L \hat{R}_{31}^{(H,k)} \frac{\mathrm{d}^2\Psi_r(x)}{\mathrm{d}x^2} \mathrm{d}x \ , \quad R_L = -\frac{1}{R_{load}} \ ,$$

$$P_D = -\int_0^L \hat{S}_{33}^{(k)} dx \ , \quad Q_q^{(u)} = \int_0^L \hat{I}^{(A,k)} \Theta_q(x) \mathrm{d}x + I_{tip}^{(A,k)} \Theta_q(L) \ , \ Q_q^{(w)} = \int_0^L \hat{I}^{(A,k)} \Psi_q(x) \mathrm{d}x + I_{tip}^{(A)} \Psi_q(L) \ ,$$

$$C_{qr}^{(u)} = \alpha_u M_{qr}^{(u)} + \beta_u K_{qr}^{(u)} \quad , C_{qr}^{(w)} = \alpha_w M_{qr}^{(w)} + \beta_w K_{qr}^{(u)} \ , \ \hat{I}^{(A,k)} = bI^{(A,k)} \ , \ \hat{I}^{(C,k)} = bI^{(C,k)} \ ,$$

$$\hat{C}_{11}^{(D,k)} = bC_{11}^{(D,k)} \quad , \hat{C}_{11}^{(F,k)} = bC_{11}^{(F,k)} \ , \quad \hat{R}_{31}^{(G,k)} = bR_{31}^{(G,k)} \quad , \quad \hat{R}_{31}^{(H,k)} = bR_{31}^{(H,k)} \quad , \quad \hat{S}_{33}^{(k)} = bS_{33}^{(k)} \ .$$

It should be noted that the ^ symbol refers to the modified variables after multiplying with the width *b* of the bimorph. Equation (25) is a non homogeneous differential dynamic equation of the piezoelectric bimorph beam with two input base-excitation. This equation can be used for modelling the piezoelectric bimorph with either series connection or parallel connection. The connections just depend on the chosen piezoelectric couplings from equations (15d), (15g), (16d) and (16g) and also the chosen internal capacitance from equations (17b) and (17c). In

addition to that, other parameters from this research such as mass moment of inertia, stiffness coefficients, piezoelectric constant and permittivity are viewed as constant values. The geometry of the piezoelectric bimorph beam must also be considered where it will affect all aspects of power harvesting performance.

4.1. Normalised Coupling Electromechanical Dynamic Equation

This section focuses on the solution of the multi-mode electromechanical dynamic equations of the piezoelectric bimorph beam with tip mass using equation (23). The solution presented here complies with the orthonormality of the Ritz eigenfunction forms [6],[30]. Equations (23) or (25) and (24) need to be modified in order to achieve the orthonormality conditions. In this case, the convergent Ritz eigenfunction forms can be stated as,

$$w_{rel}(x,t) = \sum_{r=1}^{m} c_r^{(w)} \Psi_r(x) e^{i\omega t} \quad , \quad u_{rel}(x,t) = \sum_{r=1}^{m} c_r^{(u)} \Theta_r(x) e^{i\omega t} \quad . \tag{26}$$

In terms of the only mechanical equation, equation (26) can be substituted into equation (23) to give the independent algebraic equations of the eigenvalues corresponding to the longitudinal and transverse bending form as,

$$\sum_{r=1}^{m} \left[K_{qr}^{(u)} - \omega^{(u)2} M_{qr}^{(u)} \right] c_r^{(u)} = 0 \quad , \quad \sum_{r=1}^{m} \left[K_{qr}^{(w)} - \omega^{(w)2} M_{qr}^{(w)} \right] c_r^{(w)} = 0 \, , \quad q = 1,2,....,m \, . \tag{27}$$

It should be noted that $c_r^{(u)}$ and $c_r^{(w)}$ represent the unknown Ritz coefficients for the respective longitudinal and transverse bending forms which refer to the eigenvectors in the mechanical domain. Once the Ritz coefficients are determined associated with natural frequencies, the generalized Ritz mode shapes in terms of the *r*-degree of freedoms can be formulated as,

$$\Psi_r(x) = \sum_{k=1}^{m} c_{kr}^{(w)} \Psi_k(x) \quad , \quad \Theta_r(x) = \sum_{k=1}^{m} c_{kr}^{(u)} \Theta_k(x) \quad , \qquad r = 1,2,....,m \, . \tag{28}$$

The generalised Ritz mode shapes can be normalised with respect to mass as,

$$\hat{\Psi}_r(x) = \frac{\Psi_r(x)}{\left(\int_0^L \hat{I}^{(C,k)} \left(\frac{d\Psi_r(x)}{dx} \right)^2 dx + \int_0^L \hat{I}^{(A,k)} \Psi_r(x)^2 dx + I_{tip}^{(A)} \Psi_r(L)^2 + I_{tip}^{(C)} \left(\frac{d\Psi_r}{dx}(L) \right)^2 \right)^{1/2}} \quad , \; r = 1,2,...., \; m \quad , \tag{29a}$$

$$\hat{\Theta}_r(x) = \frac{\Theta_r(x)}{\left(\int_0^L \hat{I}^{(A,k)} \Theta_r(x)^2 dx + I_{tip}^{(A)} \Theta_r(L)^2 \right)^{1/2}} \qquad r = 1,2,....,m \, . \tag{29b}$$

The normalised eigenfunction series forms in terms of the generalised space- and time-dependent functions can now be stated as,

$$w_{rel}(x,t) = \sum_{r=1}^{m} \hat{\Psi}_r(x) w_r(t) \quad , \qquad u_{rel}(x,t) = \sum_{r=1}^{m} \hat{\Theta}_r(x) u_r(t) \quad . \tag{30}$$

Corresponding to equation (23), the orthonormalisations can be proven using equation (30) and applying the orthogonality property of the mechanical dynamic equations as,

$$\int_0^L \hat{I}^{(C,k)} \frac{\mathrm{d}\hat{\Psi}_r(x)}{\mathrm{d}x} \frac{\mathrm{d}\hat{\Psi}_q(x)}{\mathrm{d}x} \mathrm{d}x + \int_0^L \hat{I}^{(A,k)} \hat{\Psi}_r(x) \hat{\Psi}_q(x) \mathrm{d}x + I_{tip}^{(A)} \hat{\Psi}_r(L) \hat{\Psi}_q(L) + I_{tip}^{(C)} \frac{\mathrm{d}\hat{\Psi}_r(L)}{\mathrm{d}x} \frac{\mathrm{d}\hat{\Psi}_q(L)}{\mathrm{d}x} = \delta_{rq} \ , \tag{31a}$$

$$\int_0^L \hat{I}^{(A,k)} \hat{\Theta}_r(x) \hat{\Theta}_q(x) \mathrm{d}x + I_{tip}^{(A)} \hat{\Theta}_r(L) \hat{\Theta}_q(L) = \delta_{rq} \ , \ \int_0^L \hat{C}_{11}^{(D,k)} \frac{\mathrm{d}\hat{\Theta}_r(x)}{\mathrm{d}x} \frac{\mathrm{d}\hat{\Theta}_q(x)}{\mathrm{d}x} \mathrm{d}x = \omega_r^{(u)2} \delta_{rq} \ , \tag{31b}$$

$$\int_0^L \hat{C}_{11}^{(F,k)} \frac{\mathrm{d}^2\hat{\Psi}_r(x)}{\mathrm{d}x^2} \frac{\mathrm{d}^2\hat{\Psi}_q(x)}{\mathrm{d}x^2} \mathrm{d}x = \omega_r^{(w)2} \delta_{rq} \ . \tag{31c}$$

where δ_{rq} is the Kronecker delta, defined as unity for $q = r$ and zero for $q \neq r$. The Rayleigh mechanical damping can be reduced in terms of orthonormalisation as,

$$C_{rq}^{(u)} = \alpha^{(u)} \delta_{rq} + \beta^{(u)} \omega_r^{(u)2} \delta_{rq} = 2\zeta_r^{(u)} \omega_r^{(u)} \delta_{rq} \ , \quad C_{rq}^{(w)} = \alpha^{(w)} \delta_{rq} + \beta^{(w)} \omega_r^{(w)2} \delta_{rq} = 2\zeta_r^{(w)} \omega_r^{(w)} \delta_{rq} \ . \tag{32}$$

In this case, although the modal mechanical damping ratios can be determined mathematically, the chosen modal mechanical damping ratios $\zeta_r^{(u)}$ and $\zeta_r^{(w)}$ were obtained here by experiment to give accurate results at the resonance frequency amplitude regions. Applying the orthonormalisations from equations (31a) to (31c) into the electromechanical piezoelectric bimorph beam equation from equation (23) gives,

$$\begin{aligned} &\ddot{u}_r(t) + 2\zeta_r^{(u)} \omega_r^{(u)} \dot{u}_r(t) + \omega_r^{(u)2} u_r(t) + P_r^{(u)} v(t) = -Q_r^{(u)} \ddot{u}_{base}(t) \\ &\ddot{w}_r(t) + 2\zeta_r^{(w)} \omega_r^{(w)} \dot{w}_r(t) + \omega_r^{(w)2} w(t) + P_r^{(w)} v(t) = -Q_r^{(w)} \ddot{w}_{base}(t) \ . \\ &\hat{P}_r^{(u)} \dot{u}_r(t) + \hat{P}_r^{(w)} \dot{w}_r(t) + P_D \dot{v}(t) + R_L v(t) = 0 \end{aligned} \tag{33}$$

It is noted that because equation (33) has been normalised due to equation (30) in terms of equations (31a)-(31c), the parameters $P_r^{(u)}, P_r^{(w)}, \hat{P}_r^{(u)}, \hat{P}_r^{(w)}, R_L, P_D, Q_r^{(u)}$ and $Q_r^{(w)}$ can be reduced as,

$$P_r^{(u)} = -\int_0^L \hat{R}_{31}^{(G,k)} \frac{\mathrm{d}\hat{\Theta}_r(x)}{\mathrm{d}x} \mathrm{d}x \ , P_r^{(w)} = \int_0^L \hat{R}_{31}^{(H,k)} \frac{\mathrm{d}^2\hat{\Psi}_r(x)}{\mathrm{d}x^2} \mathrm{d}x \ , \hat{P}_r^{(u)} = \sum_{r=0}^{m} P_r^{(u)} \ , \hat{P}_r^{(w)} = \sum_{r=0}^{m} P_r^{(w)} \ , R_L = -\frac{1}{R_{load}} \ ,$$

$$P_D = -\int_0^L \hat{S}_{33}^{(k)} \mathrm{d}x \ , \ Q_r^{(u)} = \int_0^L \hat{I}^{(A,k)} \hat{\Theta}_r(x) \mathrm{d}x + I_{tip}^{(A)} \hat{\Theta}_r(L) \ , \ Q_r^{(w)} = \int_0^L \hat{I}^{(A,k)} \hat{\Psi}_r(x) \mathrm{d}x + I_{tip}^{(A)} \hat{\Psi}_r(L) \quad .$$

Equation (33) can be solved using Laplace transforms. In this case, the multi-mode electromechanical dynamic equations of the piezoelectric bimorph system can be reduced as,

$$u_r(s) = -\frac{1}{Z(s)_r}\left[\left\{\left(s^2 + 2\zeta_r^{(w)}\omega_r^{(w)}s + \omega_r^{(w)2}\right)(sP_D + R_L) - \sum_{r=1}^{m} sP_r^{(w)2}\right\}Q_r^{(u)}\left(s^2 u_{base}(s)\right) + \sum_{r=1}^{m} sP_r^{(w)}P_r^{(u)}Q_r^{(w)}\left(s^2 w_{base}(s)\right)\right], \quad (34a)$$

$$w_r(s) = -\frac{1}{Z(s)_r}\left[\left\{\left(s^2 + 2\zeta_r^{(u)}\omega_r^{(u)}s + \omega_r^{(u)2}\right)(sP_D + R_L) - \sum_{r=1}^{m} sP_r^{(u)2}\right\}Q_r^{(w)}\left(s^2 w_{base}(s)\right) + \sum_{r=1}^{m} sP_r^{(w)}P_r^{(u)}Q_r^{(u)}\left(s^2 u_{base}(s)\right)\right], \quad (34b)$$

$$v(s) = \frac{1}{Z(s)_r}\left[\sum_{r=1}^{m}\left\{sP_r^{(w)}Q_r^{(w)}\left(s^2 + 2\zeta_r^{(u)}\omega_r^{(u)}s + \omega_r^{(u)2}\right)\left(s^2 w_{base}(s)\right)\right\} + \sum_{r=1}^{m}\left\{sP_r^{(u)}Q_r^{(u)}\left(s^2 + 2\zeta_r^{(w)}\omega_r^{(w)}s + \omega_r^{(w)2}\right)\left(s^2 u_{base}(s)\right)\right\}\right]. \quad (34c)$$

The characteristic polynomial form from equation (33) can be formulated as,

$$\begin{aligned} Z(s)_r = {} & \left(s^2 + 2\zeta_r^{(u)}\omega_r^{(u)}s + \omega_r^{(u)2}\right)\left(s^2 + 2\zeta_r^{(w)}\omega_r^{(w)}s + \omega_r^{(w)2}\right)(sP_D + R_L) \\ & - \sum_{r=1}^{m} sP_r^{(w)2}\left(s^2 + 2\zeta_r^{(u)}\omega_r^{(u)}s + \omega_r^{(u)2}\right) - \sum_{r=1}^{m} sP_r^{(u)2}\left(s^2 + 2\zeta_r^{(w)}\omega_r^{(w)}s + \omega_r^{(w)2}\right). \end{aligned} \quad (34d)$$

4.2. Multi-mode Electromechanical Frequency Analysis

Corresponding to equations (34a)-(34c), the electromechanical dynamic equation of the piezoelectric bimorph can be formulated into FRF forms. The first multi-mode FRF represents the generalised frequency dependent longitudinal function per unit input base longitudinal excitation. In the case when input transverse excitation is ignored, the FRF due to input base longitudinal excitation can be modified as a function of position of the piezoelectric element (x) and frequency $(j\omega)$ by transforming it back into the Ritz eigenfunction form as,

$$H_{11}(x, j\omega) = \left.\frac{u_{rel}(x, j\omega)}{-\omega^2 u_{base}\, e^{j\omega t}}\right|_{s=j\omega} = -\sum_{r=1}^{m}\left[\frac{\hat{\Theta}_r(x)}{\omega_r^{(u)2} - \omega^2 + j2\zeta_r^{(u)}\omega_r^{(u)}\omega}\left(\frac{(j\omega P_D + R_L)Q_r^{(u)} - \sum_{r=1}^{m}\frac{j\omega P_r^{(w)2}Q_r^{(u)}}{\omega_r^{(w)2} - \omega^2 + j2\zeta_r^{(w)}\omega_r^{(w)}\omega}}{j\omega P_D + R_L - \sum_{r=1}^{m}\frac{j\omega P_r^{(w)2}}{\omega_r^{(w)2} - \omega^2 + j2\zeta_r^{(w)}\omega_r^{(w)}\omega} - \sum_{r=1}^{m}\frac{j\omega P_r^{(u)2}}{\omega_r^{(u)2} - \omega^2 + j2\zeta_r^{(u)}\omega_r^{(u)}\omega}}\right)\right]. \quad (35)$$

The FRF of the relative transfer function between the input base transverse acceleration and output longitudinal displacement can be obtained as,

$$H_{12}(x, j\omega) = \left.\frac{u_{rel}(x, j\omega)}{-\omega^2 w_{base}\, e^{j\omega t}}\right|_{s=j\omega} = -\sum_{r=1}^{m}\left[\frac{\hat{\Theta}_r(x)}{\omega_r^{(u)2} - \omega^2 + j2\zeta_r^{(u)}\omega_r^{(u)}\omega}\left(\frac{\sum_{r=1}^{m}\frac{j\omega P_r^{(u)}P_r^{(w)}Q_r^{(w)}}{\omega_r^{(w)2} - \omega^2 + j2\zeta_r^{(w)}\omega_r^{(w)}\omega}}{j\omega P_D + R_L - \sum_{r=1}^{m}\frac{j\omega P_r^{(w)2}}{\omega_r^{(w)2} - \omega^2 + j2\zeta_r^{(w)}\omega_r^{(w)}\omega} - \sum_{r=1}^{m}\frac{j\omega P_r^{(u)2}}{\omega_r^{(u)2} - \omega^2 + j2\zeta_r^{(u)}\omega_r^{(u)}\omega}}\right)\right]. \quad (36)$$

The second multi-mode FRF represents the transverse motion with respect to input motions. If base-input transverse motion is ignored, the FRF of transverse motion related to the base input longitudinal motion can be obtained as,

$$H_{21}(x, j\omega) = \left.\frac{w_{rel}(x, j\omega)}{-\omega^2 u_{base}\, e^{j\omega t}}\right|_{s=j\omega} = -\sum_{r=1}^{m}\left[\frac{\hat{\Psi}_r(x)}{\omega_r^{(w)2} - \omega^2 + j2\zeta_r^{(w)}\omega_r^{(w)}\omega}\left(\frac{\sum_{r=1}^{m}\frac{j\omega P_r^{(u)}P_r^{(w)}Q_r^{(u)}}{\omega_r^{(u)2} - \omega^2 + j2\zeta_r^{(u)}\omega_r^{(u)}\omega}}{j\omega P_D + R_L - \sum_{r=1}^{m}\frac{j\omega P_r^{(w)2}}{\omega_r^{(w)2} - \omega^2 + j2\zeta_r^{(w)}\omega_r^{(w)}\omega} - \sum_{r=1}^{m}\frac{j\omega P_r^{(u)2}}{\omega_r^{(u)2} - \omega^2 + j2\zeta_r^{(u)}\omega_r^{(u)}\omega}}\right)\right]. \quad (37)$$

The multi-mode FRF of transverse displacement with respect to input base transverse acceleration can be obtained as,

$$H_{22}(x,j\omega)=\left.\frac{w_{rel}(x,j\omega)}{-\omega^2 w_{base}\ e^{j\omega t}}\right|_{s=j\omega}=-\sum_{r=1}^{m}\left[\frac{\hat{\Psi}_r(x)}{\omega_r^{(w)2}-\omega^2+\ j2\zeta_r^{(w)}\omega_r^{(w)}\omega}\left(\frac{(j\omega P_D+R_L)Q_r^{(w)}-\sum_{r=1}^{m}\frac{j\omega P_r^{(u)2}Q_r^{(w)}}{\omega_r^{(u)2}-\omega^2+\ j2\zeta_r^{(u)}\omega_r^{(u)}\omega}}{j\omega P_D+R_L-\sum_{r=1}^{m}\frac{j\omega P_r^{(w)2}}{\omega_r^{(w)2}-\omega^2+\ j2\zeta_r^{(w)}\omega_r^{(w)}\omega}-\sum_{r=1}^{m}\frac{j\omega P_r^{(u)2}}{\omega_r^{(u)2}-\omega^2+\ j2\zeta_r^{(u)}\omega_r^{(u)}\omega}}\right)\right]. \quad (38)$$

The FRF between output electric voltage and the input base longitudinal acceleration can be obtained as,

$$H_{31}(j\omega)=\left.\frac{v(j\omega)}{-\omega^2 u_{base}e^{j\omega t}}\right|_{s=j\omega}=\frac{\sum_{r=1}^{m}\frac{j\omega P_r^{(u)}Q_r^{(u)}}{\omega_r^{(u)2}-\omega^2+\ j2\zeta_r^{(u)}\omega_r^{(u)}\omega}}{j\omega P_D+R_L-\sum_{r=1}^{m}\frac{j\omega P_r^{(w)2}}{\omega_r^{(w)2}-\omega^2+\ j2\zeta_r^{(w)}\omega_r^{(w)}\omega}-\sum_{r=1}^{m}\frac{j\omega P_r^{(u)2}}{\omega_r^{(u)2}-\omega^2+\ j2\zeta_r^{(u)}\omega_r^{(u)}\omega}}. \quad (39)$$

The multi-mode FRF of the electric voltage output with respect to the input base transverse excitation can be calculated, omitting the input base longitudinal excitation to give,

$$H_{32}(j\omega)=\left.\frac{v(j\omega)}{-\omega^2 w_{base}e^{j\omega t}}\right|_{s=j\omega}=\frac{\sum_{r=1}^{m}\frac{j\omega P_r^{(w)}Q_r^{(w)}}{\omega_r^{(w)2}-\omega^2+\ j2\zeta_r^{(w)}\omega_r^{(w)}\omega}}{j\omega P_D+R_L-\sum_{r=1}^{m}\frac{j\omega P_r^{(w)2}}{\omega_r^{(w)2}-\omega^2+\ j2\zeta_r^{(w)}\omega_r^{(w)}\omega}-\sum_{r=1}^{m}\frac{j\omega P_r^{(u)2}}{\omega_r^{(u)2}-\omega^2+\ j2\zeta_r^{(u)}\omega_r^{(u)}\omega}}. \quad (40)$$

The multi-mode FRF of the electric current output related to the input base longitudinal acceleration can be obtained as,

$$H_{41}(j\omega)=\left.\frac{I(j\omega)}{-\omega^2 u_{base}e^{j\omega t}}\right|_{s=j\omega}=\frac{\frac{1}{R_{load}}\sum_{r=1}^{m}\frac{j\omega P_r^{(u)}Q_r^{(u)}}{\omega_r^{(u)2}-\omega^2+\ j2\zeta_r^{(u)}\omega_r^{(u)}\omega}}{j\omega P_D+R_L-\sum_{r=1}^{m}\frac{j\omega P_r^{(w)2}}{\omega_r^{(w)2}-\omega^2+\ j2\zeta_r^{(w)}\omega_r^{(w)}\omega}-\sum_{r=1}^{m}\frac{j\omega P_r^{(u)2}}{\omega_r^{(u)2}-\omega^2+\ j2\zeta_r^{(u)}\omega_r^{(u)}\omega}}. \quad (41)$$

The FRF of the electric current output related to the input base transverse excitation can be calculated, omitting the input base longitudinal excitation to give,

$$H_{42}(j\omega)=\left.\frac{I(j\omega)}{-\omega^2 w_{base}e^{j\omega t}}\right|_{s=j\omega}=\frac{\frac{1}{R_{load}}\sum_{r=1}^{m}\frac{j\omega P_r^{(w)}Q_r^{(w)}}{\omega_r^{(w)2}-\omega^2+\ j2\zeta_r^{(w)}\omega_r^{(w)}\omega}}{j\omega P_D+R_L-\sum_{r=1}^{m}\frac{j\omega P_r^{(w)2}}{\omega_r^{(w)2}-\omega^2+\ j2\zeta_r^{(w)}\omega_r^{(w)}\omega}-\sum_{r=1}^{m}\frac{j\omega P_r^{(u)2}}{\omega_r^{(u)2}-\omega^2+\ j2\zeta_r^{(u)}\omega_r^{(u)}\omega}}. \quad (42)$$

The multi-mode FRF of power harvesting related to the longitudinal acceleration can be expressed as,

$$\left.\frac{P(j\omega)}{\left(-\omega^2 u_{base}e^{j\omega t}\right)^2}\right|_{s=j\omega} = \left[\frac{\frac{1}{\sqrt{R_{load}}}\sum_{r=1}^{m}\frac{j\omega P_r^{(u)}Q_r^{(u)}}{\omega_r^{(u)2}-\omega^2+j2\zeta_r^{(u)}\omega_r^{(u)}\omega}}{j\omega P_D+R_L-\sum_{r=1}^{m}\frac{j\omega P_r^{(w)2}}{\omega_r^{(w)2}-\omega^2+j2\zeta_r^{(w)}\omega_r^{(w)}\omega}-\sum_{r=1}^{m}\frac{j\omega P_r^{(u)2}}{\omega_r^{(u)2}-\omega^2+j2\zeta_r^{(u)}\omega_r^{(u)}\omega}}\right]^2. \quad (43)$$

The multi-mode FRF of power harvesting related to the transverse acceleration can be calculated as,

$$\left.\frac{P(j\omega)}{\left(-\omega^2 w_{base}e^{j\omega t}\right)^2}\right|_{s=j\omega} = \left[\frac{\frac{1}{\sqrt{R_{load}}}\sum_{r=1}^{m}\frac{j\omega P_r^{(w)}Q_r^{(w)}}{\omega_r^{(w)2}-\omega^2+j2\zeta_r^{(w)}\omega_r^{(w)}\omega}}{j\omega P_D+R_L-\sum_{r=1}^{m}\frac{j\omega P_r^{(w)2}}{\omega_r^{(w)2}-\omega^2+j2\zeta_r^{(w)}\omega_r^{(w)}\omega}-\sum_{r=1}^{m}\frac{j\omega P_r^{(u)2}}{\omega_r^{(u)2}-\omega^2+j2\zeta_r^{(u)}\omega_r^{(u)}\omega}}\right]^2. \quad (44)$$

The optimal multi-mode FRF of power harvesting related to the transverse acceleration can be calculated by differentiating with respect to load resistance and setting the differentiable power function to zero. It is noted that parameter R_L represents per-unit load resistance $-1/R_{load}$. Corresponding to equation (44), the optimal load resistance can be formulated as,

$$R_{load}^{opt} = \frac{\sqrt{X(\omega)^2+Y(\omega)^2}}{X(\omega)^2+Y(\omega)^2}, \quad (45)$$

where,

$$X(\omega)=\omega P_D-\sum_{r=1}^{m}\frac{\omega P_r^{(w)2}\left(\omega_r^{(w)2}-\omega^2\right)}{\left(\omega_r^{(w)2}-\omega^2\right)^2+\left(2\zeta_r^{(w)}\omega_r^{(w)}\omega\right)^2}-\sum_{r=1}^{m}\frac{\omega P_r^{(u)2}\left(\omega_r^{(u)2}-\omega^2\right)}{\left(\omega_r^{(u)2}-\omega^2\right)^2+\left(2\zeta_r^{(u)}\omega_r^{(u)}\omega\right)^2},$$

$$Y(\omega)=\sum_{r=1}^{m}\frac{\omega P_r^{(w)2}\left(2\zeta_r^{(w)}\omega_r^{(w)}\omega\right)}{\left(\omega_r^{(w)2}-\omega^2\right)^2+\left(2\zeta_r^{(w)}\omega_r^{(w)}\omega\right)^2}-\sum_{r=1}^{m}\frac{\omega P_r^{(u)2}\left(2\zeta_r^{(u)}\omega_r^{(u)}\omega\right)}{\left(\omega_r^{(u)2}-\omega^2\right)^2+\left(2\zeta_r^{(u)}\omega_r^{(u)}\omega\right)^2}.$$

It should be noted that the optimal load resistance can be substituting back into equation (44) to give the optimal power harvesting. Corresponding to equations (30b), (35) and (36), modifying equation (34a) in terms of the generalised time-dependent longitudinal function and any position along the piezoelectric beam gives the steady state relative longitudinal displacement under two input base excitations as,

$$u_{rel}(x,t)=H_{11}(x,j\omega)\left(-\omega^2 u_{base}e^{j\omega t}\right)+H_{12}(x,j\omega)\left(-\omega^2 w_{base}e^{j\omega t}\right). \quad (46)$$

The multi-mode absolute longitudinal displacement can be formulated in terms of equation (46) as,

$$u_{abs}(x,t)=u_{base}e^{j\omega t}+H_{11}(x,j\omega)\left(-\omega^2 u_{base}e^{j\omega t}\right)+H_{12}(x,j\omega)\left(-\omega^2 w_{base}e^{j\omega t}\right). \quad (47)$$

It should be noted that the absolute displacement fields have been discussed at the beginning of this paper in terms of the kinematic diagram of the beam where equation (47) was formulated as $u_{abs}(x,t)=u_{base}(t)+u_{rel}(x,t)$. The steady state relative transverse motion in equation (34b) in terms of any position on the piezoelectric beam can be modified corresponding with equations (30a), (37) and (38) as,

$$w_{rel}(x,t)=H_{21}(x,j\omega)\left(-\omega^2 u_{base}e^{j\omega t}\right)+H_{22}(x,j\omega)\left(-\omega^2 w_{base}e^{j\omega t}\right). \tag{48}$$

Corresponding to equation (48), the multi-mode absolute transverse displacement can be reduced as,

$$w_{abs}(x,t)=\ w_{base}e^{j\omega t}\ +H_{21}(x,j\omega)\left(-\omega^2 u_{base}e^{j\omega t}\right)+H_{22}(x,j\omega)\left(-\omega^2 w_{base}e^{j\omega t}\right). \tag{49}$$

It should be noted that equation (49) is formulated according to the kinematics of the bimorph beam as discussed previously to give $w_{abs}(x,t)=w_{base}(t)+w_{rel}(x,t)$. Equation (34c) can be modified to the generalised electrical potential response in terms of equations (39) and (40) to give,

$$v(t)=H_{31}(j\omega)\left(-\omega^2 u_{base}e^{j\omega t}\right)+H_{32}(j\omega)\left(-\omega^2 w_{base}e^{j\omega t}\right)\ . \tag{50}$$

It should be noted that u_{base} and w_{base} refer to the input base longitudinal and transverse displacement excitations on the bimorph. Corresponding to equations (47) and (49), equations (35) and (38) can be modified to give the multi-mode FRF of the absolute displacements and velocities related to the base input longitudinal and transverse accelerations at any position along the bimorph respectively as,

$$\begin{aligned}
&\hat{H}_{11}^{(disp)}(x,j\omega)=\frac{u_{base}e^{j\omega t}+u_{rel}(x,t)}{-\omega^2 u_{base}e^{j\omega t}}=-\frac{1}{\omega^2}+H_{11}(x,j\omega)\ ,\quad \hat{H}_{11}^{(vel)}(x,j\omega)=\frac{\frac{d}{dt}\left[u_{base}e^{j\omega t}+u_{rel}(x,t)\right]}{-\omega^2 u_{base}e^{j\omega t}}=\frac{1}{j\omega}+\ j\omega H_{11}(x,j\omega),\\
&\hat{H}_{22}^{(disp)}(x,j\omega)=\frac{w_{base}e^{j\omega t}+w_{rel}(x,t)}{-\omega^2 w_{base}e^{j\omega t}}=-\frac{1}{\omega^2}+H_{22}(x,j\omega)\ ,\ \hat{H}_{22}^{(vel)}(x,j\omega)=\frac{\frac{d}{dt}\left[w_{base}e^{j\omega t}+w_{rel}(x,t)\right]}{-\omega^2 w_{base}e^{j\omega t}}=\frac{1}{j\omega}+\ j\omega H_{22}(x,j\omega).
\end{aligned} \tag{51}$$

It should be noted that equations (47), (49) and (51) are applicable for analysing the absolute dynamic responses when comparing the results using the Laser Doppler Vibrometer (LDV) because the signal output from the Vibrometer can be transferred into a digital signal FFT Analyzer to display the results. The results obtained from measurements were the time dependent absolute displacement, velocity, acceleration and frequency response function located at any position along the piezoelectric bimorph beam.

5. Closed Form Method of the Normalised Coupling Electromechanical Dynamic Equation

This section focuses on the multi-mode frequency response using the closed form of the electromechanical dynamic equations under two input base excitations. The closed-form analytical method was formulated according to the strong form of the Hamiltonian principle which was formulated from equations (20a) to (22). This included the electromechanical bimorph element with the boundary-value problem where the partial differential equations associated with the geometry and natural boundary conditions were formulated from those equations. The solution form from this analytical method involves the space- and time-dependence of convergent eigenfunction forms which can be formulated as

$$w_{rel}(x,t) = \sum_{r=1}^{\infty} \hat{\Psi}_r(x) w_r(t) \quad , \quad u_{rel}(x,t) = \sum_{r=1}^{\infty} \hat{\Theta}_r(x) u_r(t) \quad . \tag{52}$$

It should be noted that equation (52) is sometimes called the mode superposition theorem which utilizes the normalised mode shapes and generalised time dependent coordinates. It should be noted that space-dependent eigenfunction forms of the Euler-Bernoulli piezoelectric bimorph for closed-form method are given in appendices A and B. At this point, the equation considering the coupled electromechanical longitudinal and transverse forms of the piezoelectric element can be further formulated in terms of frequency analysis. As formulated in equations (20a) and (21a), the boundary-value problem formulated for the piezoelectric bimorph element can be expressed using the normalised eigenfunction series under two input base excitations. The first representation of the electromechanical piezoelectric bimorph under transverse bending from equation (21a) can be reformulated using equation (52a) and multiplying with $\hat{\Psi}_q(x)$, the results obtained can be further integrated with respect to x gives as,

$$\int_0^L \hat{I}^{(A,k)} \hat{\Psi}_r(x) \hat{\Psi}_q(x) \ddot{w}_r(t) \mathrm{d}x - \int_0^L \hat{I}^{(C,k)} \frac{\mathrm{d}^2 \hat{\Psi}_r(x)}{\mathrm{d}x^2} \hat{\Psi}_q(x) \ddot{w}_r(t) \mathrm{d}x$$

$$+ \int_0^L \hat{C}_{11}^{(F,k)} \frac{\mathrm{d}^2}{\mathrm{d}x^2} \left(\frac{\mathrm{d}^2 \hat{\Psi}_r(x)}{\mathrm{d}x^2} \right) \hat{\Psi}_q(x) w_r(t) \mathrm{d}x + \int_0^L \hat{I}^{(A,k)} \hat{\Psi}_q(x) \ddot{w}_{base} \mathrm{d}x = 0 \, . \tag{53}$$

The boundary conditions from equation (21b) can be further formulated by substituting equation (52a) as,

$$\hat{\Psi}_r(0,t) = 0 \quad , \quad \frac{\mathrm{d}\hat{\Psi}_r(0,t)}{\mathrm{d}x} = 0 \quad , \tag{54}$$

and two dynamic boundary conditions can be further formulated as,

$$-I_{tip}^{(A)}\ddot{w}_{base} - I_{tip}^{(A)}\hat{\Psi}_r(L)\ddot{w}_r(t) + \hat{C}_{11}^{(F,k)}\frac{\mathrm{d}}{\mathrm{d}x}\left(\frac{\mathrm{d}^2\hat{\Psi}_r(L)}{\mathrm{d}x^2}\right)w_r(t) - \hat{I}^{(C,k)}\frac{\mathrm{d}\hat{\Psi}_r}{\mathrm{d}x}(L)\ddot{w}_r(t) = 0, \quad (55)$$

$$-\hat{I}_{tip}^{(C)}\frac{\mathrm{d}\hat{\Psi}_r(L)}{\mathrm{d}x}\ddot{w}_r(t) - \hat{C}_{11}^{(F,k)}\frac{\mathrm{d}^2\hat{\Psi}_r(L)}{\mathrm{d}x^2}w_r(t) - \hat{R}_{31}^{(H,k)}v(t) = 0. \quad (56)$$

In terms of the orthogonality relations, the second and third terms of equation (53) can be further manipulated by using partial integration and then applying equations (54)-(56). The result of which can be used to reformulate equation (53) as,

$$\int_0^L \hat{I}^{(A,k)}\hat{\Psi}_r(x)\hat{\Psi}_q(x)\mathrm{d}x\ddot{w}_r(t) + I_{tip}^{(A)}\hat{\Psi}_r(L)\hat{\Psi}_q(L)\ddot{w}_r(t) + I_{tip}^{(C)}\frac{\mathrm{d}\hat{\Psi}_r(L)}{\mathrm{d}x}\frac{\mathrm{d}\hat{\Psi}_q(L)}{\mathrm{d}x}\ddot{w}_r(t)$$

$$+\int_0^L \hat{C}_{11}^{(F,k)}\frac{\mathrm{d}^2\hat{\Psi}_r(x)}{\mathrm{d}x^2}\frac{\mathrm{d}^2\hat{\Psi}_q(x)}{\mathrm{d}x^2}\mathrm{d}x w_r(t) + \int_0^L \hat{I}^{(C,k)}\frac{\mathrm{d}\hat{\Psi}_r(x)}{\mathrm{d}x}\frac{\mathrm{d}\hat{\Psi}_q(x)}{\mathrm{d}x}\mathrm{d}x\ddot{w}_r(t) + \hat{R}_{31}^{(H,k)}\frac{\mathrm{d}\hat{\Psi}_q(L)}{\mathrm{d}x}v(t)$$

$$= -\int_0^L \hat{I}^{(A,k)}\hat{\Psi}_q(x)\mathrm{d}x\ddot{w}_{base} - I_{tip}^{(A)}\hat{\Psi}_q(L)\ddot{w}_{base}. \quad (57)$$

It should be noted that the normalised eigenfunction series in equation (52a) also must meet the orthogonality relations to correctly represent the mode shapes. As mentioned previously, this section gives the piezoelectric bimorph beam equations based on Rayleigh's beam assumption as it considers the rotary inertia of the bimorph beam. The Euler-Bernoulli bimorph beam can be formulated by ignoring the rotary inertia of the bimorph beam. In this case, the normalised mass from equation (58a) can be used to ignore the rotary inertia of the bimorph beam at the first integration to give the typical Euler-Bernoulli bimorph beam condition. The orthonormalisations can be provided by using equation (52a) and applying the orthogonality property of the mechanical dynamic equations as,

$$\int_0^L \hat{I}^{(C,k)}\frac{\mathrm{d}\hat{\Psi}_r(x)}{\mathrm{d}x}\frac{\mathrm{d}\hat{\Psi}_q(x)}{\mathrm{d}x}\mathrm{d}x + \int_0^L \hat{I}^{(A,k)}\hat{\Psi}_r(x)\hat{\Psi}_q(x)\mathrm{d}x + I_{tip}^{(A)}\hat{\Psi}_r(L)\hat{\Psi}_q(L) + I_{tip}^{(C)}\frac{\mathrm{d}\hat{\Psi}_r(L)}{\mathrm{d}x}\frac{\mathrm{d}\hat{\Psi}_q(L)}{\mathrm{d}x} = \delta_{rq}, \quad (58a)$$

$$\int_0^L \hat{C}_{11}^{(F,k)}\frac{\mathrm{d}^2\hat{\Psi}_r(x)}{\mathrm{d}x^2}\frac{\mathrm{d}^2\hat{\Psi}_q(x)}{\mathrm{d}x^2}\mathrm{d}x = \omega_r^{(w)2}\delta_{rq} \quad . \quad (58b)$$

where δ_{rq} is the Kronecker delta, defined as unity for $q = r$ and zero for $q \neq r$. It should be noted that equations (58a) and (58b) represent specific orthogonality conditions based on the boundary conditions. The mechanical damping based on Rayleigh's principle can be reduced in terms of orthonormality as,

$$C_{rq}^{(w)} = \alpha^{(w)}\delta_{rq} + \beta^{(w)}\omega_r^{(w)2}\delta_{rq} = 2\zeta_r^{(w)}\omega_r^{(w)}\delta_{rq}. \quad (59)$$

Equation (59) can now be reformulated by including Rayleigh's damping coefficient according to orthogonality conditions as,

$$\ddot{w}_r(t) + 2\zeta_r^{(w)}\omega_r^{(w)}\dot{w}_r(t) + \omega_r^{(w)2} w(t) + P_r^{(w)} v(t) = -Q_r^{(w)}\ddot{w}_{base}(t) \quad . \tag{60}$$

The second case of the electromechanical dynamic equation associated with boundary conditions represents the electromechanical piezoelectric bimorph under longitudinal extension. Here it is formulated using equation (20a) corresponding to equation (52b) and multiplying with $\hat{\Theta}_q(x)$, the result obtained can be integrated with respect to x to give,

$$-\int_0^L \hat{I}^{(A,k)}\hat{\Theta}_r(x)\hat{\Theta}_q(x)\ddot{u}_r \mathrm{d}x - \int_0^L \hat{I}^{(A,k)}\hat{\Theta}_q(x)\ddot{u}_{base}(t)\mathrm{d}x + \int_0^L \hat{C}_{11}^{(D,k)}\hat{\Theta}_q(x)\frac{\mathrm{d}^2\hat{\Theta}_r(x)}{\mathrm{d}x^2}u_r \mathrm{d}x = 0\,. \tag{61}$$

The boundary conditions from equation (20b) can be further formulated by substituting equation (52b) as,

$$\hat{\Theta}_r(0,t)=0, \quad -I_{tip}^{(A)}\ddot{u}_{base}(t) - I_{tip}^{(A)}\hat{\Theta}_r(L)\ddot{u}_r - \hat{C}_{11}^{(D,k)}\frac{\mathrm{d}\hat{\Theta}_r(L)}{\mathrm{d}x}u_r + \hat{R}_{31}^{(G,k)}v(t) = 0\,. \tag{62}$$

In terms of orthogonality relations, the third term of equation (61) can be further manipulated by using the partial integral form and then applying equation (62). The result of which can used to reformulate equation (61) to give,

$$\int_0^L \hat{I}^{(A,k)}\hat{\Theta}_r(x)\hat{\Theta}_q(x)\ddot{u}_r \mathrm{d}x + I_{tip}^{(A)}\hat{\Theta}_r(L)\hat{\Theta}_q(L)\ddot{u}_r + \int_0^L \hat{C}_{11}^{(D,k)}\frac{\mathrm{d}\hat{\Theta}_r(x)}{\mathrm{d}x}\frac{\mathrm{d}\hat{\Theta}_q(x)}{\mathrm{d}x}u_r \,\mathrm{d}x - \hat{R}_{31}^{(G,k)}\hat{\Theta}_q(L)v(t)$$
$$= -\int_0^L \hat{I}^{(A,k)}\hat{\Theta}_q(x)\ddot{u}_{base}(t)\mathrm{d}x - I_{tip}^{(A)}\hat{\Theta}_q(L)\ddot{u}_{base}(t)\,. \tag{63}$$

In this case, the second part of the normalised eigenfunction series in equation (52b) also must meet the orthogonality relations in order to correctly specify the longitudinal mode shapes. Furthermore, the specific orthogonality condition based on equation (63) can be established as,

$$\int_0^L \hat{I}^{(A,k)}\hat{\Theta}_r(x)\hat{\Theta}_q(x)\mathrm{d}x + I_{tip}^{(A)}\hat{\Theta}_r(L)\hat{\Theta}_q(L) = \delta_{rq} \;,\; \int_0^L \hat{C}_{11}^{(D,k)}\frac{\mathrm{d}\hat{\Theta}_r(x)}{\mathrm{d}x}\frac{\mathrm{d}\hat{\Theta}_q(x)}{\mathrm{d}x}\mathrm{d}x = \omega_r^{(u)2}\delta_{rq}\,, \tag{64}$$

where δ_{rq} is the Kronecker delta, defined as unity for $q = r$ and zero for $q \neq r$. The mechanical damping constant based on Rayleigh's principle can be reduced in terms of orthonormality as,

$$C_{rq}^{(u)} = \alpha^{(u)}\delta_{rq} + \beta^{(u)}\omega_r^{(u)2}\delta_{rq} = 2\zeta_r^{(u)}\omega_r^{(u)}\delta_{rq}\,. \tag{65}$$

Equation (63) can now be reformulated by including Rayleigh's damping coefficient based on the orthonormality conditions as,

$$\ddot{u}_r(t) + 2\zeta_r^{(u)}\omega_r^{(u)}\dot{w}_r(t) + \omega_r^{(u)2} w(t) + P_r^{(u)} v(t) = -Q_r^{(u)}\ddot{u}_{base}(t)\,. \tag{66}$$

The third case of the electromechanical dynamic equation from equation (22) represents the piezoelectric bimorph under electrical form. Equation (22) can be modified by substituting

equation (52) into equation (22) and differentiating it with respect to time to obtain the parameters of velocity and electrical current gives,

$$\sum_{r=1}^{\infty}\int_{0}^{L}\hat{R}_{31}^{(G,k)}\frac{\mathrm{d}\hat{\Theta}_r(x)}{\mathrm{d}x}\mathrm{d}x\dot{u}_r(t)-\sum_{r=1}^{\infty}\int_{0}^{L}\hat{R}_{31}^{(H,k)}\frac{\mathrm{d}^2\hat{\Psi}_r(x)}{\mathrm{d}x^2}\mathrm{d}x\dot{w}_r(t)+\int_{0}^{L}\hat{S}_{33}^{(k)}\mathrm{d}x\dot{v}(t)+\frac{1}{R_{load}}v(t)=0\,. \tag{67}$$

The equation (67) can be reformulated as,

$$\sum_{r=1}^{\infty}\hat{P}_r^{(u)}\dot{u}_r(t)+\sum_{r=1}^{\infty}\hat{P}_r^{(w)}\dot{w}_r(t)+P_D\dot{v}(t)+R_Lv(t)=0\,. \tag{68}$$

In this case, the electromechanical piezoelectric bimorph beam based on equations (60), (66) and (68) can be reformulated to give,

$$\begin{aligned}
&\ddot{u}_r(t)+2\zeta_r^{(u)}\omega_r^{(u)}\dot{u}_r(t)+\omega_r^{(u)2}u_r(t)+P_r^{(u)}v(t)=-Q_r^{(u)}\ddot{u}_{base}(t)\\
&\ddot{w}_r(t)+2\zeta_r^{(w)}\omega_r^{(w)}\dot{w}_r(t)+\omega_r^{(w)2}w(t)+P_r^{(w)}v(t)=-Q_r^{(w)}\ddot{w}_{base}(t)\\
&\sum_{r=1}^{\infty}\hat{P}_r^{(u)}\dot{u}_r(t)+\sum_{r=1}^{\infty}\hat{P}_r^{(w)}\dot{w}_r(t)+P_D\dot{v}(t)+R_Lv(t)=0
\end{aligned}\,. \tag{69}$$

It can be noted that because equation (69) has been normalised due to equations (58a), (58b), and (64), the parameters $P_r^{(u)}$, $P_r^{(w)}$, $\hat{P}_r^{(u)}$, $\hat{P}_r^{(w)}$, P_D, R_L, $Q_r^{(u)}$ and $Q_r^{(w)}$ can be reduced as,

$$P_r^{(u)}=-\hat{R}_{31}^{(G,k)}\hat{\Theta}_r(L)\,,\quad P_r^{(w)}=\hat{R}_{31}^{(H,k)}\frac{\mathrm{d}\hat{\Psi}_r(L)}{\mathrm{d}x}\,,\quad P_D=\int_{0}^{L}\hat{S}_{33}^{(k)}\mathrm{d}x\,,$$

$$\sum_{r=1}^{\infty}\hat{P}_r^{(u)}=\sum_{r=1}^{\infty}\int_{0}^{L}\hat{R}_{31}^{(G,k)}\frac{\mathrm{d}\hat{\Theta}_r(x)}{\mathrm{d}x}\mathrm{d}x\,,\quad \sum_{r=1}^{\infty}\hat{P}_r^{(w)}=-\sum_{r=1}^{\infty}\int_{0}^{L}\hat{R}_{31}^{(H,k)}\frac{\mathrm{d}^2\hat{\Psi}_r(x)}{\mathrm{d}x^2}\mathrm{d}x\,,$$

$$R_L=\frac{1}{R_{load}}\,,\quad Q_r^{(u)}=\int_{0}^{L}\hat{I}^{(A,k)}\hat{\Theta}_r(x)\mathrm{d}x+I_{tip}^{(A)}\hat{\Theta}_r(L)\,,\quad Q_r^{(w)}=\int_{0}^{L}\hat{I}^{(A,k)}\hat{\Psi}_r(x)\mathrm{d}x+I_{tip}^{(A)}\hat{\Psi}_r(L)\,.$$

It is clear that equation (69) provides the closed-form of electromechanical dynamic equations with two input base motions and this equation can be further formulated using Laplace transformations to give the multi-mode electromechanical dynamic equations of the piezoelectric bimorph. Equations (69) and (33) appear to be similar to each other but have different sign and operation for some parameters. It should be noted that the electromechanical closed-form method can give accurate results because of its convergence for the chosen frequency response mode of interest. In comparison with the electromechanical weak form solution based on the Ritz analytical approach method, the typical mode shapes or space-independent eigenfunction forms and number of modes must be chosen correctly in order to meet convergence criteria and give results similar to the closed-form method. For example, the FRFs results from the analytical weak form as discussed in the next section only show the first mode but were iterated using three modes of interest to give accurate results. In this case, the

weak form was chosen, having the same typical space-independent eigenfunctions (appendices A and B) as for the closed-form to reduce computational time and number of iterations to meet the speedy convergence criteria.

6. Theoretical and Experimental Results

The suggested formulations in terms of the electromechanical dynamic responses of the piezoelectric bimorph beam under two input base longitudinal and transverse excitations are used here for comparison with experimental results. The list of properties of the bimorph used in this investigation is given in Table 2. Figure 6 shows the experimental setup. The piezoelectric bimorph beam with the tip mass was clamped at the protractor base structure with the given input base acceleration in order to investigate the effects of electromechanical dynamic responses of the bimorph. The B & K impedance head type 8001 was connected to the B & K Charge Amplifier Type 2635 to measure the input acceleration from the B & K exciter type 4809. The wave function generator, connected to the B & K Power Amplifier Type 2706, was used to control the harmonic forcing frequency of the exciter. Moreover, the laser digital vibrometer Polytec PDV 100 was focused on reflector tape attached to the tip mass in order to measure the time-dependent dynamic displacement, velocity and also frequency response. In this case, all signal measurements from the charge amplifier, piezoelectric bimorph and vibrometer were connected to the B & K FFT pulse Analyzer 3560B. The reduced single mode FRFs with varying load resistances can be used to model the electromechanical piezoelectric bimorph of the electrical parallel connection. The sinusoidal base input acceleration of cantilevered piezoelectric bimorph was 306 mg equivalent to 3 m/s^2 (1 g = gravitational acceleration 9.81 m/s^2). The generalised time-dependent dynamic response along the length of the bimorph was measured using the laser vibrometer. The absolute dynamic velocity FRFs from the theoretical analysis can then be used for comparison with the experimental results.

As can be seen from Figure 7, the trend of the tip absolute dynamic velocity FRFs at the first resonance frequency shifts when the load resistance changes. As can be seen, the weak and closed form analytical methods indicated good agreement with experimental results. The highest amplitude was achieved at short and open circuit load resistances of 560 Ω at frequency of 76.1 Hz and 602 kΩ at frequency of 79.6 Hz respectively. The effect of load resistance on the piezoelectric bimorph can be viewed as resistive shunt damping effect resulting in shifting of the resonant frequency as shown clearly in Figure 8. It is important to

notice here that although the bimorph FRF analysis changed from the short and open circuit load resistances, the mechanical behaviour was predominantly affected by the resonance frequency behaviour. It is also noted that since the piezoelectric element has profound internal mechanical and electrical effects, the piezoelectric couplings and internal capacitance also affects the frequency domain as indicated by the electromechanical damping and stiffness. As proved theoretically, the forward and backward piezoelectric couplings were created as a result of electrical force and moment due to the direct and converse mode thermopiezoelectric behaviour.

Figure 9 shows the trend of electrical voltage FRFs with variable load resistance using the weak and close form analytical methods where the results showed good agreement with experiment. As also seen, the frequency response shifts as the load resistance changes where the resonance amplitude increases from short to open circuit load resistances. It is clearly seen from the three dimensional graph in Figure 10 that the region of maximum electrical voltage amplitude located at the open circuit load resistance gradually decreased to the minimum level at the short circuit load resistance followed by a shift in frequency. By considering the electrical current as shown in Figure 11, the trend seems opposite to that of the electrical voltage where the lowest frequency of 76.1 Hz with short circuit load resistance seemed to give the highest amplitude. The amplitude then decreased to the lowest value at the load resistance approaching open circuit followed by the increasing resonance at 79.6 Hz. This was also clearly seen in Figure 12 where the maximum current amplitude dropped dramatically when the load resistance increased from short circuit. In the next section, further explanation in given by considering the relationship of electromechanical responses between velocity, voltage, current and power.

In this section, the weak and closed forms of the analytical power harvesting FRF as shown in Figure 13 were found to give good agreement with the experimental results. The trend of power response as a function of load resistance can be compared with the previous trends of tip absolute velocity, electric voltage and current. The minimum current amplitude occurred at the open circuit load resistance with maximum amplitudes of tip absolute velocity and maximum electric voltage response at a resonance frequency of 79.6 Hz. Conversely, the maximum current amplitude was obtained at the short circuit load resistance with the maximum amplitude of tip absolute velocity with decreasing voltage amplitude at the resonance frequency of 76.1 Hz. This shows that the electrical current increased when the load resistance approached short

circuit, but the tip absolute velocity of the bimorph tended to give the highest amplitude. This indicates that this situation would be unsuitable for power harvester optimization.

As expected, the highest tip absolute velocity amplitude did not result in the highest power harvesting with short circuit resistance. The electrical current FRF for the short circuit load resistance gave the highest amplitude whereas the electric voltage response indicated the highest amplitude for open circuit load resistance. In fact, the power harvesting under the short or open circuit is not preferred due to the lower amplitudes. This can be seen clearly from Figure 14 where the maximum power amplitude region was achieved at the load resistance away from short and open circuits. The sensitivity of the bimorph to generate the optimal power harvesting shows the importance of understanding the underlying strain-polarity field on the piezoelectric element from the bimorph under variable load resistance. The convenient electrical power amplitude would be from an intermediate curve of load resistance of 60 kΩ where this value indicated the lowest tip absolute velocity amplitude around the resonance frequency of 77.83 Hz but showed convenient values for voltage, current and optimal power harvesting. The optimal power can be seen with the black triangular curve in Figure 13 representing the optimal load resistance where the high amplitude coincidently overlapped with the load resistance of 60 kΩ. Two local maximum points from the optimal load resistance curve also coincidently overlapped with the load resistances of 20 kΩ and 200 kΩ, respectively. It should be noted that both local minimum and maximum points indicated optimal power harvesting with very small differences in value. If we consider the local maximum points of 20 kΩ and 200 kΩ by comparing with the local minimum point, the local maximum points of 20 kΩ can provide lower voltage and higher current compared with the local minimum point of 60 kΩ. Conversely, local maximum points of 200 kΩ seemed to give higher voltage and lower current compared with the local minimum point of 60 kΩ. It is also noted that the velocity amplitude with load resistance of 60 kΩ above the resonance frequency of 77.83 Hz indicated lower value than load resistance of 200 kΩ and higher value than load resistance of 20 kΩ but with small differences in value. Conversely, the velocity amplitude with load resistance of 60 kΩ below the resonance frequency of 77.83 Hz indicated higher value than the load resistance of 200 kΩ but with small differences in value and lower value than load resistance of 20 kΩ. The power harvesting with the load resistance of 60 kΩ showed the best response for the optimization covering the broadest frequency range.

7. Conclusion

This paper has presented the development of novel analytical methods for modelling the electromechanical dynamic equations for one and two input base excitations of the piezoelectric bimorph beam with tip mass using the Rayleigh and Euler-Bernoulli's beam assumptions. The Rayleigh piezoelectric bimorph beam only considers the second mass moment of inertia (rotary) of the bimorph where this can also be reduced to the Euler-Bernoulli's piezoelectric bimorph beam by ignoring the beam rotary inertia. The strong form of the Hamiltonian's principle under series and parallel connections was also presented. The weak form derived from strong form represents the analytical approach developed using the Ritz method whereas the closed form derived from strong form can be further formulated using the direct analytical solution with orthonormalisation by introducing the space- and time-dependent eigenfunction series into boundary conditions. The accuracy of the closed-form solution over the frequency response domain is based on the convergence at any particular mode of interest derived using analytical methods. Corresponding to the convergence criteria, the weak form associated with the correct chosen typical mode shapes and number of modes also gives good agreement with the closed form. The effect of strain field due to transverse bending and longitudinal extension affects not only the mechanical moment and force of all layers of the bimorph but also the electrical moment and force of the top and bottom piezoelectric layers of the bimorph. Concerning the electrical moment and force, the backward and forward piezoelectric couplings due to the transverse and longitudinal forms can also be formulated, where these give the electromechanical coupling of the piezoelectric layers. Furthermore, the weak form of the electromechanical dynamic equations were further formulated using the orthonormality conditions to obtain the coupled electromechanical dynamic response of transverse-longitudinal form to give the multi-mode frequency response functions (FRFs) using Laplace transforms. The closed form of the electromechanical dynamic equations in terms of orthonormality conditions were also formulated. The multi-input dynamic excitation and multi-output electromechanical dynamic responses have been formulated. As a result, the validations between the analytical weak and closed forms and experimental results were achieved with good agreement where the single mode, reduced from multi-mode FRFs, was the main concern for power harvesting. The results obtained from single mode FRFs showed the changes in resonance frequency based on the load resistance changes. As also shown, the short and open circuit load resistances were not suitable conditions for optimising power harvesting. This has been linked to other parameters where the maximum voltage occurred at the open circuit load resistance whereas the maximum current was found at the

load resistances approaching short circuit. Moreover, the maximum level of tip absolute velocity of the bimorph was achieved at the short and open circuit load resistances which gave the lowest power amplitudes.

Appendix A. Determining the space-dependent eigenfunction form of the Euler-Bernoulli piezoelectric bimorph beam with tip mass

Since the piezoelectric bimorph beam is a cantilevered system, the characteristic mechanical dynamic equation in transverse bending beam form can be formulated as,

$$\frac{\mathrm{d}^4\Psi_r(x)}{\mathrm{d}x^4} - \mu^4\Psi_r(x) = 0 \quad . \tag{A1}$$

Four distinct roots can be obtained as,

$$\lambda_{1,2} = \pm\mu \quad , \quad \lambda_{3,4} = \pm j\mu \quad . \tag{A2}$$

where $\mu^4 = \hat{I}^{(A,k)}\omega^2/\hat{C}_{11}^{(F,k)}$. The boundary condition of the cantilevered piezoelectric beam with the tip mass and rotary moment of inertia from the tip mass can be formulated as,

$$\hat{C}_{11}^{(F,k)}\frac{\mathrm{d}^2\Psi_r}{\mathrm{d}x^2}(L) - I_{tip}^{(C)}\omega^2\frac{\mathrm{d}\Psi_r}{\mathrm{d}x}(L) = 0\,, \tag{A3}$$

$$\hat{C}_{11}^{(F,k)}\frac{\mathrm{d}^3\Psi_r}{\mathrm{d}x^3}(L) + I_{tip}^{(A)}\omega^2\Psi_r(L) = 0\,, \tag{A4}$$

$$\Psi_r(0) = 0 \quad , \quad \frac{\mathrm{d}\Psi_r}{\mathrm{d}x}(0) = 0\,. \tag{B5}$$

The characteristic equation can be obtained after manipulating Eqs. (A1) - (A5) to give,

$$\begin{bmatrix} A_{11} & A_{12} \\ A_{21} & A_{22} \end{bmatrix}\begin{Bmatrix} c_1 \\ c_4 \end{Bmatrix} = 0 \quad , \tag{A6}$$

where,

$$A_{11} = -\left(\cos(\mu L) + \cosh(\mu L)\right) + \frac{I_{tip}^{(C)}\mu^3}{\hat{I}^{(A,k)}}\left(\sin(\mu L) + \sinh(\mu L)\right)$$

$$A_{12} = \left(\sin(\mu L) + \sinh(\mu L)\right) + \frac{I_{tip}^{(C)}\mu^3}{\hat{I}^{(A,k)}}\left(\cos(\mu L) - \cosh(\mu L)\right)$$

$$A_{21} = \left(\sin(\mu L) - \sinh(\mu L)\right) + \frac{I_{tip}^{(A)}\mu}{\hat{I}^{(A,k)}}\left(\cos(\mu L) - \cosh(\mu L)\right)$$

$$A_{22} = \left(\cos(\mu L) + \cosh(\mu L)\right) - \frac{I_{tip}^{(A)}\mu}{\hat{I}^{(A,k)}}\left(\sin(\mu L) - \sinh(\mu L)\right)$$

The frequency equation and eigenvalues can be calculated by analysing the determinant from Eq. (A6) to give,

$$\left(1 + \cos(\mu L)\cosh(\mu L)\right) - \frac{I_{tip}^{(C)}\mu^3}{\hat{I}^{(A,k)}}\left(\cos\mu L\sinh\mu L + \sin\mu L\cosh\mu L\right)$$

$$+\frac{I_{tip}^{(A)}\mu}{\hat{I}^{(A,k)}}\left(\cos\mu L\sinh\mu L-\sin\mu L\cosh\mu L\right)+\frac{I_{tip}^{(A)}I_{tip}^{(C)}\mu^4}{\hat{I}^{(A,k)^2}}\left(1-\cos\mu L\cosh\mu L\right)=0\,. \qquad \text{(A7)}$$

After applying boundary conditions and some algebraic calculations, the mode shape or space-dependent eigenfunction can now be formulated as,

$$\Psi_r(x)=c_{1r}\left(\cos(\mu x)-\cosh(\mu x)+\frac{\mathrm{A}_{21}}{\mathrm{A}_{22}}\left(\sin(\mu x)-\sinh(\mu x)\right)\right)\quad . \qquad \text{(A8)}$$

Appendix B. Determining the space-dependent Longitudinal eigenfunction form of the piezoelectric bimorph beam with tip mass

To formulate the space-dependent eigenfunction form, the characteristic dynamic equation of longitudinal motion for the cantilevered piezoelectric bimorph beam can be written as,

$$\frac{\mathrm{d}^2\Theta(x)}{\mathrm{d}x^2}+\gamma^2\Theta(x)=0\ . \qquad \text{(B1)}$$

Equation (B1) can be modified into a characteristic equation and two roots from the characteristic equation can be obtained as,

$$\lambda_{1,2}=\pm j\gamma \quad \text{where}, \quad \gamma^2=\frac{\omega^2\,\hat{I}^{(A,k)}}{\hat{C}_{11}^{(D,k)}}\quad . \qquad \text{(B2)}$$

The boundary condition can be formulated as,

$$\hat{C}_{11}^{(D,k)}\frac{\mathrm{d}\Theta}{\mathrm{d}x}(L)-I_{tip}^{(A)}\omega^2\Theta(L)=0\quad ,\quad \Theta(0)=0\ . \qquad \text{(B3)}$$

The frequency equation and eigenvalues can be calculated by applying boundary conditions to give,

$$\tan\gamma L=\frac{\hat{C}_{11}^{(D,k)}\gamma}{I_{tip}^{(A)}\omega^2}\quad . \qquad \text{(B4)}$$

After applying boundary conditions and some algebraic calculations, the space-dependent eigenfunction form can now be formulated as

$$\Theta_r(x)=b_{1r}\sin\gamma x\ . \qquad \text{(B5)}$$

References

[1] B. J. Chen, Z. M. Xiao and K. M. Liew, *Electro-elastic stress analysis for a wedge-shaped crack interacting with a screw dislocation in piezoelectric solid*, Int. J. Eng. Sci. 40 (2002) pp. 621 – 635, 2002.

[2] Z. M. Xiao and J. Bai, *Numerical simulation on a coated piezoelectric sensor interacting with a crack*, Finite. Elem. Analy. Design, 38 (2002), pp. 691-706.

[3] C.-P.Fritzen and P.Kraemer, *Self-diagnosis of smart structures based on dynamical properties*, Mech. Sys. Signal Processing 23 (2009), pp. 1830–1845.

[4] D. Guyomar, S.Mohammadi and C.Richard, *Effect of boundary (support) conditions on piezoelectric damping in the case of SSDI vibration control technique*, Mech. Sys. Signal Processing 23 (2009), pp. 501-513.
[5] N.S. Hudak and G.G. Amatucci, *Small-scale energy harvesting through thermoelectric, vibration, and radiofrequency power conversion*, J. Appl. Phys. 103 **(**2008), pp. 101301.
[6] M.F. Lumentut, *Mathematical Dynamics of Electromechanical Piezoelectric Energy Harvesters*, Ph.D. diss., Curtin University, Australia, 2011.
[7] C.G. Knight, *Wireless networks : Implications for aircraft loads monitoring*, Defence Science and Technology Organisation, Australian Department of Defence (2007), DSTO-TN-0759.
[8] S. Priya, *Advances in energy harvesting using low profile piezoelectric transducers*, J. Electroceramic. 19 (2007), pp.167-184.
[9] K.A. Cook-Chennault, N. Thambi, M.A. Bitetto and E.B. Hameyie, *Piezoelectric energy harvesting*, Bullet. Sci.Technol. Soc. 28 (2008), pp. 496-509.
[10] S. Roundy, P. Wright and J. Rabaey, *A study of low level vibrations as a power source for wireless sensor nodes*, Comp. Communi. 26 (2003), pp. 1131–1144.
[11] J.G. Smits and W.-S. Choi, *The constituent equations of piezoelectric heterogeneous bimorphs*, *IEEE Trans. Ultraso. Ferroelec. Freq. Control*, 46 (1991), pp. 256–269.
[12] Q.-M. Wang, X.-H. Du, B. Xu and L.E. Eric Cross, *Theoretical analysis of the sensor effect of cantilever piezoelectric benders*, J. Appl. Phys. 85 (1999) ,pp. 1702-1712.
[13] S. Roundy and P.K. Wright, *A piezoelectric vibration based generator for wireless electronics*, Smart Mater.Struct. 18 (2004), pp. 1131–1142.
[14] N.E. duToit, B.L. Wardle and S.-G. Kim, *Design considerations for MEMS-scale piezoelectric mechanical vibration energy harvesters*, J. Integr. Ferroelectr. 71 (2005), pp. 121-160.
[15] Y.C. Shu and I.C. Lien, *Analysis of power output for piezoelectric energy harvesting systems*, Smart Mater.Struct. 15 (2006), pp.1499-1512.
[16] A. Erturk and D.J. Inman, *An experimentally validated bimorph cantilevered model for Piezoelectric energy harvesting from base excitations*, Smart Mater. Struct.19 **(**2009), pp. 1-18.
[17] F. Goldschmidtboeing and P. Woias, *Characterization of different beam shapes for piezoelectric energy harvesting*, J. Micromech. Microeng. 18 (2008), pp. 104013.
[18] M.L. Friswell and S. Adhikari, *Sensor shape design for piezoelectric cantilever beams to harvest vibration energy*, J. Appl. Phys.108 **(**2010), pp. 014901.
[19] C. Sun, J. Shi and X. Wang, *Fundamental study of mechanical energy harvesting using piezoelectric nanostructures*, J. Appl. Phys. 108 (2010), pp. 034309.
[20] T. Harigai, H. Adachi and E. Fujii E, *Vibration energy harvesting using highly (001)-oriented Pb(Zr,Ti)O3 thin film*, J. Appl. Phys. 107 (2010), pp. 096101.
[21] M.F. Lumentut and I.M. Howard, *An analytical method for vibration modelling of a piezoelectric bimorph beam for power harvesting*, Proc. ASME conf. on Smart Mater. Adaptive Struct. Intell. Syst. Oxnard, California, USA, 19-23 September, 2009, pp. 601-611.
[22] M.F. Lumentut and I.M. Howard, *The analysis of a piezoelectric bimorph beam with two input base motions for Power harvesting*, IOP Conf. Series: Mater. Sci. Eng. 10 (2010), pp. 012169.
[23] M.F. Lumentut and I.M. Howard, *The experimental validation of an electromechanical dynamic model of a piezoelectric bimorph beam for prediction of power generation*, Proc. 6th Australasian Cong. on Applied Mechanics, 2010.
[24] J.F. Nye *Physical Properties of Crystals: Their Representation by Tensors and Matrices*, Clarendon Press, Oxford, England, 1985.
[25] H.F. Tiersten, *Linear Piezoelectric Plate Vibrations*, Plenum Press, 1969.

[26] H. Tanaka, *Generalized basic equations for bending motions of piezoelectric bars formulated from Hamilton's principle*, J. Acoustic. Soc. Am. 4 (1993), pp. 1764-1772.
[27] T. Ikeda, *Fundamentals of Piezoelectricity*, Oxford Science Publishing, New York, 1990.
[28] J.G. Smits, S.I. Dalke and T.K. Cooney, *The constituent equations of piezoelectric bimorphs*, Sens. Actuators A : Phys. 28 **(**1991), pp. 41–61.
[29] F.P. Beer and E.R. Johnston, *Vector Mechanics for Engineers: Statics and Dynamics* McGraw-Hill, USA, 1977.
[30] W. Ritz, *Über eine neue Methode zur Lösung gewisser Variationprobleme der Mathematischen Physik*, J. Reine Angew. Math. 135 (1909), pp. 1–61.

Table 1 Summary of three different types of power generators.

Type	Advantages	Disadvantages
Piezoelectric	no external voltage no mechanical stop high power density high output voltage high sensitivity compatible with MEMS	depolarisation brittleness of piezoceramic materials high impedance
Electromagnetic	no external voltage no mechanical stop	difficult to integrate with MEMS low output voltage low sensitivity bulky size from the magnet and coil
Electrostatic	compatible with MEMS	need external voltage complex design for plate capacitor comb low power density need mechanical stop

Table 2 Characteristic properties of the piezoelectric bimorph system.

Material properties	**Piezoelectric**	**Brass**	**Geometry properties**	**Piezoelectric**	**Brass**
Young's modulus , $\overline{Q}_{11}$ (GPa)	66	105	Length , L (mm)	30.1	30.1
Density, ρ (kg/m^3)	7800	9000	Thickness, h (mm)	0.19 (each)	0.13
Piezoelectric constant, d_{31} (pm/V)	-190	-	Width, b (mm)	6.4	6.4
Permittivity, ς_{33}^{T} (F/m)	$1800\,\varsigma_o$	-	First coefficient $I_{tip}^{(A)}$ (kg)†	0.0022	
permittivity of free space, ς_o (pF/m)	8.854	-	Third coefficient $I_{tip}^{(C)}$ (kg m^2)†	7.3743×10^{-9}	

† Calculated according to the geometry and material properties of tip mass and the rotary inertia at centre of gravity of tip mass coincident with the end of the bimorph length. First and third coefficients refer to zeroth and second mass moment of inertias respectively.

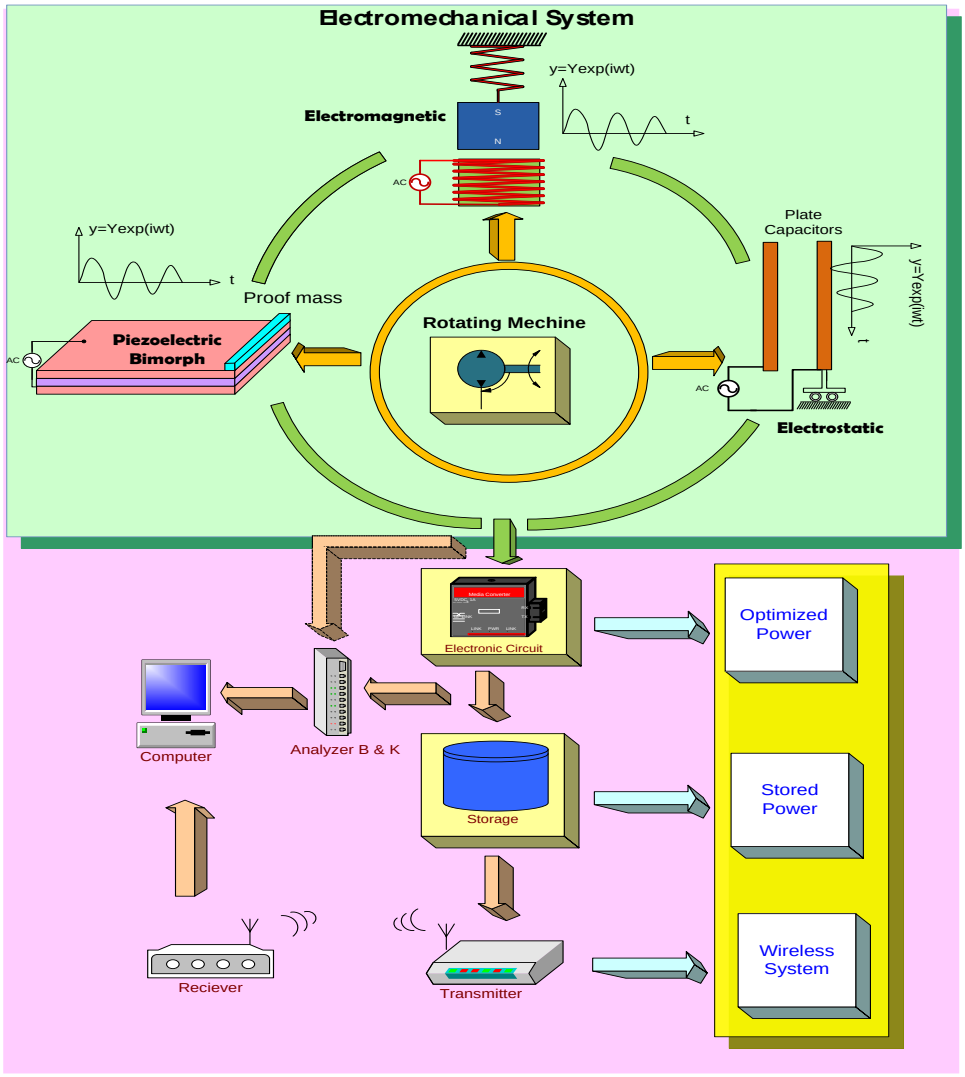

Figure 1 Schematic of Electromechanical Power Harvesting System.

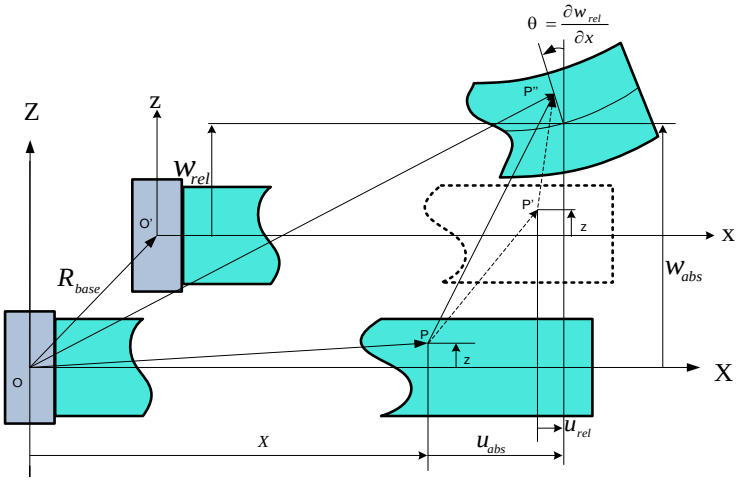

Figure 2. Kinematic motion of the Piezoelectric Bimorph Beam

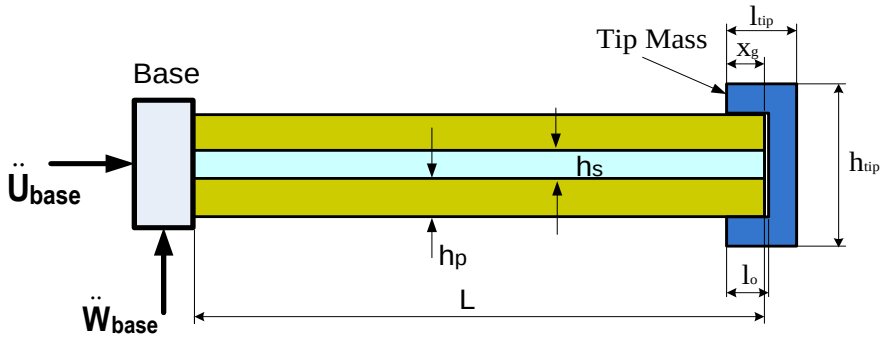

Figure 3. Piezoelectric Bimorph Beam with a Tip Mass

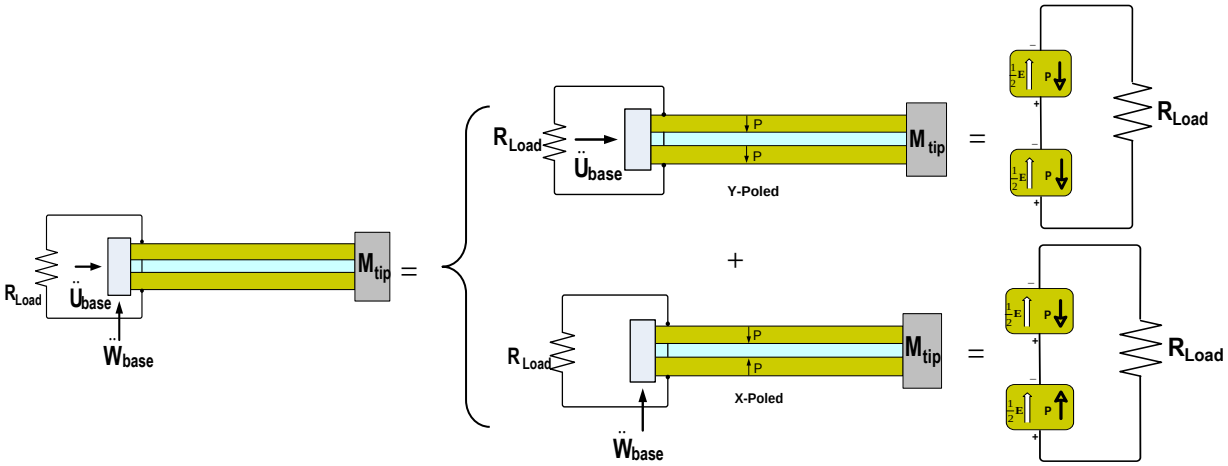

Figure 4. Cantilevered piezoelectric bimorph beam with two input base longitudinal and transverse excitations under series connections

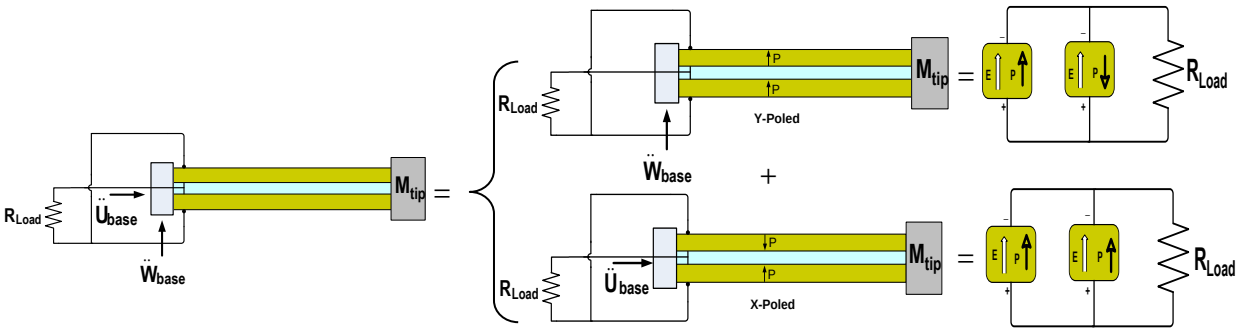

Figure 5. Cantilevered piezoelectric bimorph beam with two input base longitudinal and transverse excitations under parallel connections

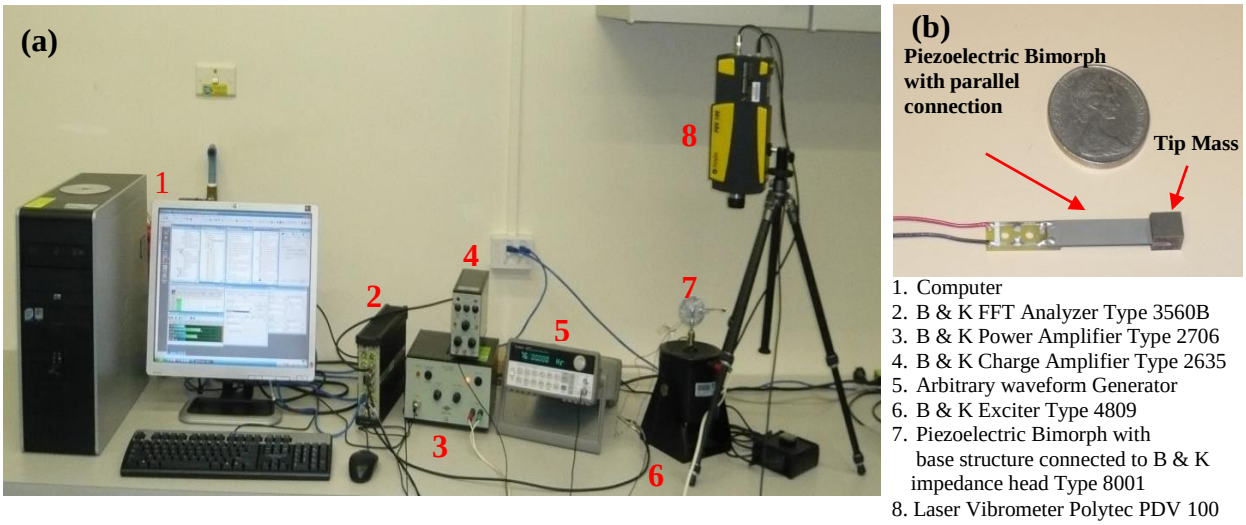

1. Computer
2. B & K FFT Analyzer Type 3560B
3. B & K Power Amplifier Type 2706
4. B & K Charge Amplifier Type 2635
5. Arbitrary waveform Generator
6. B & K Exciter Type 4809
7. Piezoelectric Bimorph with base structure connected to B & K impedance head Type 8001
8. Laser Vibrometer Polytec PDV 100

Figure 6. (a) Experimental Setup and (b) Piezoelectric bimorph beam with tip mass under parallel connection

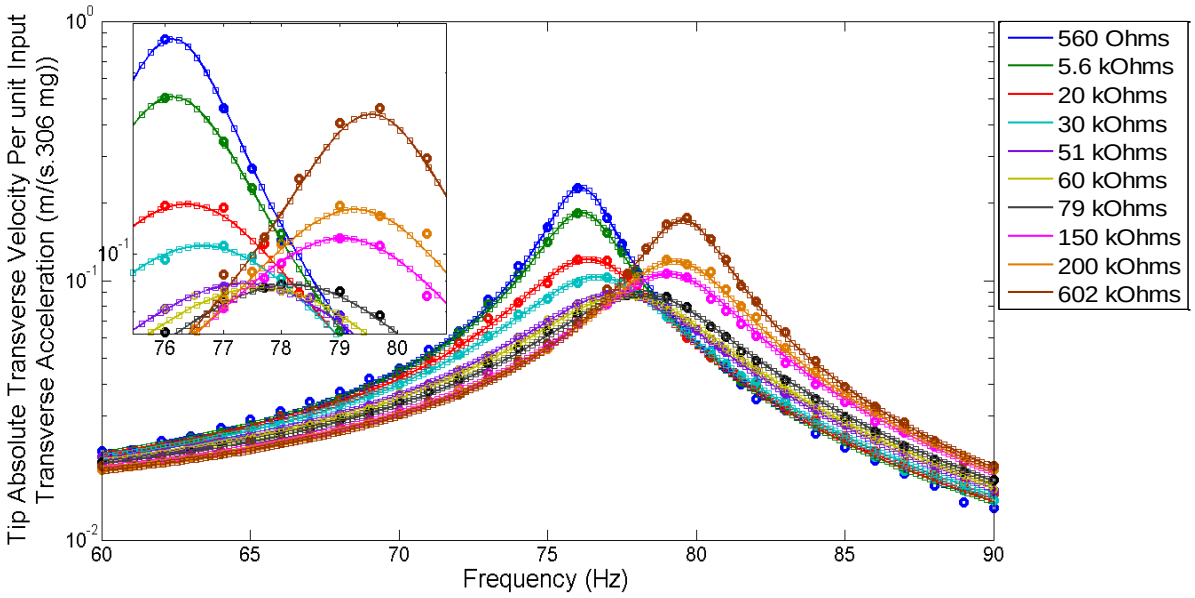

Figure 7. FRFs of tip absolute Dynamic Velocity : Analytical Weak form (Solid line), Analytical Closed form (Square line) and Experiment (Round dot)

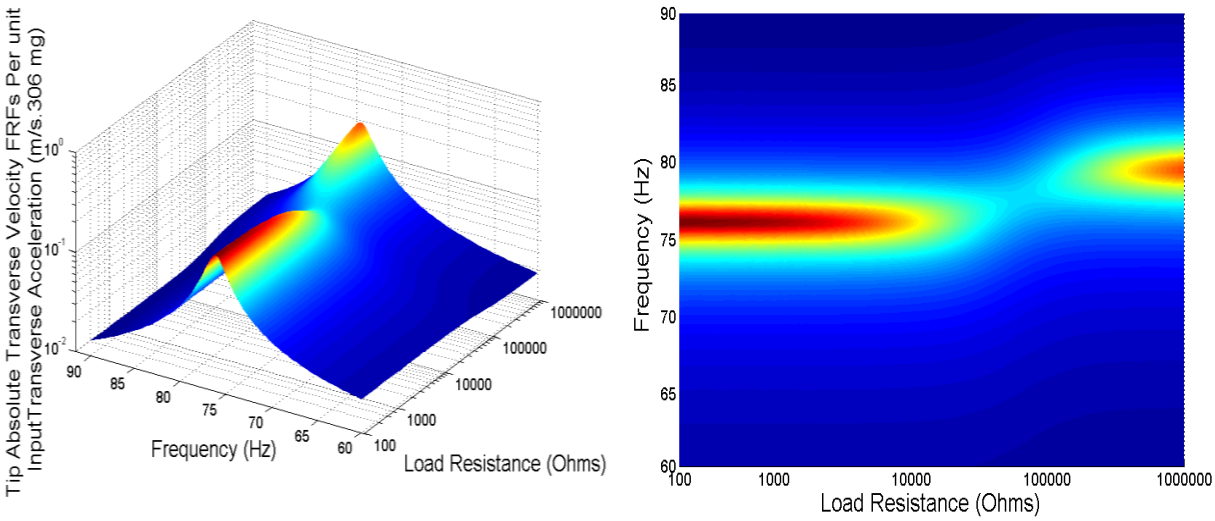

Figure 8. FRFs of tip absolute Dynamic Velocity: a) Amplitude Vs Frequency and Load resistance, b) Amplitude Pattern based on: Frequency Vs Load resistance

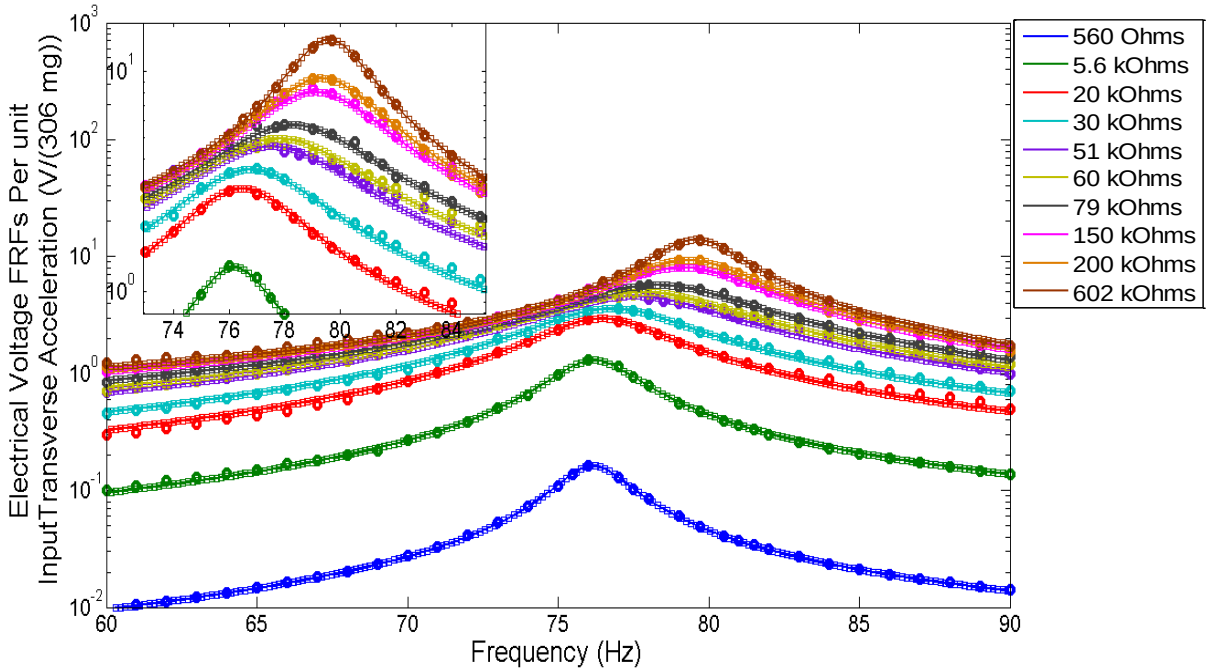

Figure 9. FRFs of Electrical Voltage : Analytical Weak form (Solid line), Analytical Closed form (Square line) and Experiment (Round dot)

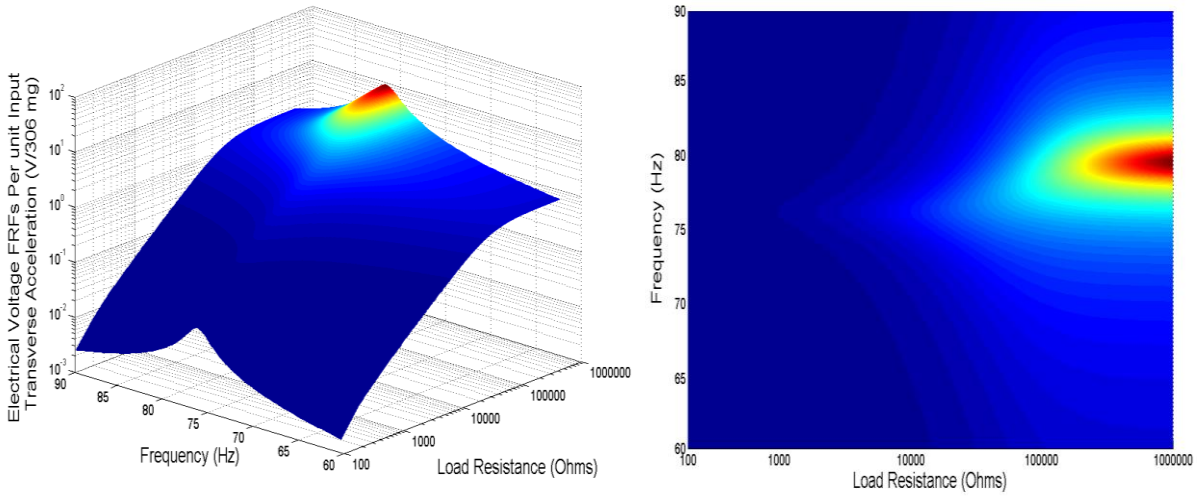

Figure 10. FRFs of Electrical Voltage : a) Amplitude Vs Frequency and Load resistance , b) Amplitude Pattern based on: Frequency Vs Load resistance

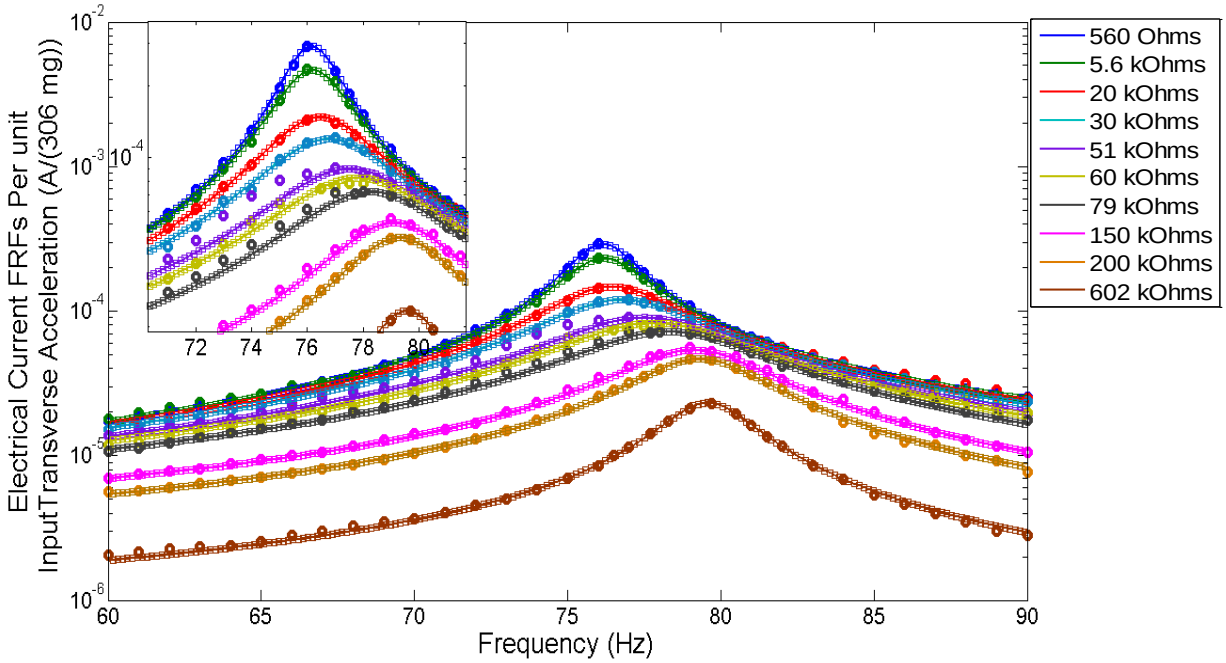

Figure 11. FRFs of Electrical Current : Analytical Weak form (Solid line), Analytical Closed form (Square line) and Experiment (Round dot)

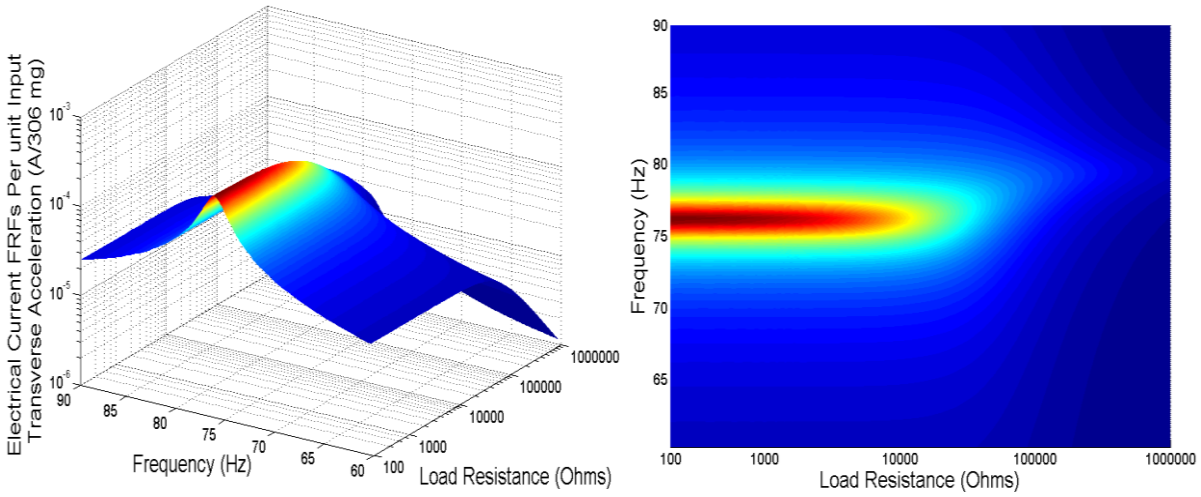

Figure 12. FRFs of Electrical Current : a) Amplitude Vs Frequency and Load resistance , b) Amplitude Pattern based on: Frequency Vs Load resistance

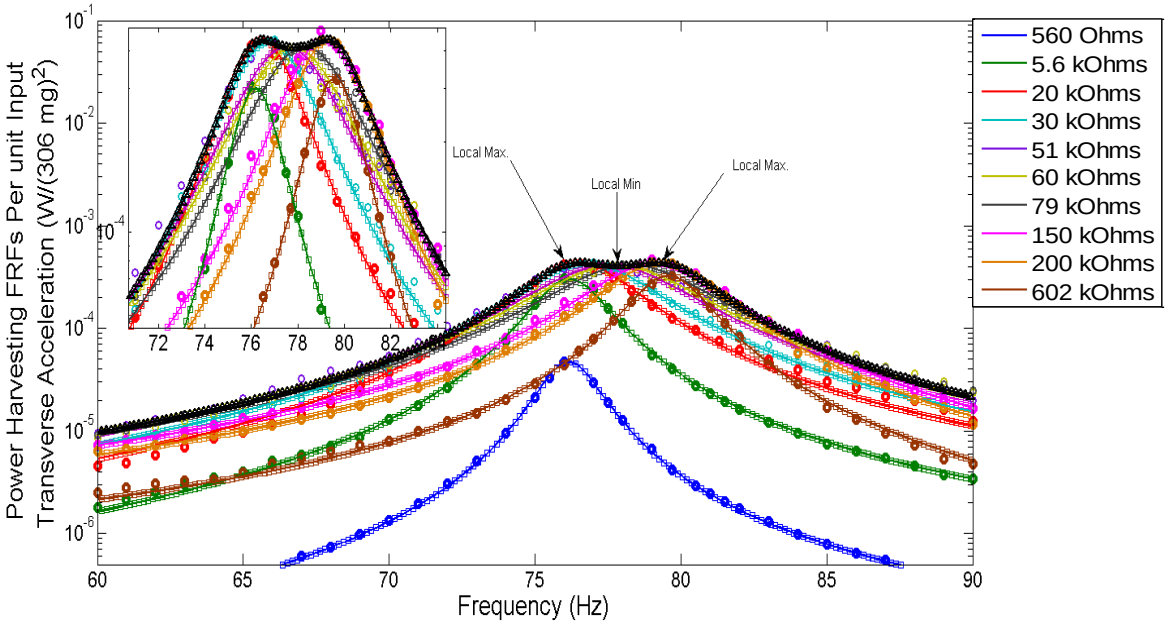

Figure 13. FRFs of Electrical Power : Analytical Weak form (Solid line), Analytical Closed form (Square line) and Experiment (Round dot)

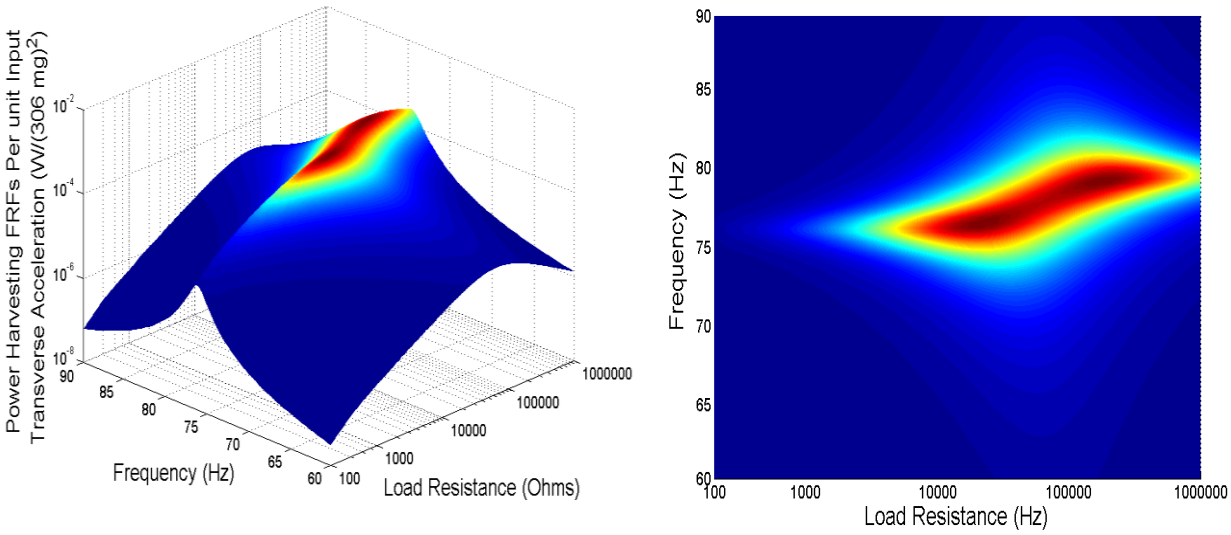

Figure 14. FRFs of Electrical Power: a) Amplitude Vs Frequency and Load resistance, b) Amplitude Pattern based on: Frequency Vs Load resistance